U–Pb detrital zircon geochronology and source provenance in the Moroccan Meseta (Variscan belt): A perspective from the Rehamna massif

Mehdi Jouhari, Francis Chopin, Mohamed El Houicha, Jean-François Ghienne, Karel Schulmann, Jitka Míková, Michel Corsini

▶ **To cite this version:**

Mehdi Jouhari, Francis Chopin, Mohamed El Houicha, Jean-François Ghienne, Karel Schulmann, et al.. U–Pb detrital zircon geochronology and source provenance in the Moroccan Meseta (Variscan belt): A perspective from the Rehamna massif. Journal of African Earth Sciences, 2022, 194, pp.104610. ⟨10.1016/j.jafrearsci.2022.104610⟩. ⟨hal-03841054⟩

HAL Id: hal-03841054

https://hal.science/hal-03841054v1

Submitted on 6 Nov 2022

HAL is a multi-disciplinary open access archive for the deposit and dissemination of scientific research documents, whether they are published or not. The documents may come from teaching and research institutions in France or abroad, or from public or private research centers.

L'archive ouverte pluridisciplinaire **HAL**, est destinée au dépôt et à la diffusion de documents scientifiques de niveau recherche, publiés ou non, émanant des établissements d'enseignement et de recherche français ou étrangers, des laboratoires publics ou privés.

HAL Authorization

U–Pb detrital zircon geochronology and source provenance in the Moroccan Meseta (Variscan belt): a perspective from the Rehamna massif

Mehdi JOUHARI[1,2], Francis CHOPIN[1,2*], Mohamed EL HOUICHA[3], Jean-François GHIENNE[1], Karel SCHULMANN[1,2], Jitka MÍKOVÁ[4], Michel CORSINI[5]

[1] Institut Terre et Environnement de Strasbourg, UMR 7063, Université de Strasbourg, CNRS – France

[2] Centre for Lithospheric Research, Czech Geological Survey – Czech Republic

[3] LGG, Faculté des Sciences, Université Chouaïb Doukkali, El Jadida – Morocco

[4] Laboratories of the Czech Geological Survey, Prague – Czech Republic

[5] Géoazur UMR 6526, Université Côte d'Azur – France

*Corresponding author: Francis Chopin

Keywords

Detrital zircon geochronology, Rehamna, Moroccan Variscan belt, Paleozoic

Abstract

Metasandstones from early Cambrian to early Carboniferous stratigraphic successions were sampled in the Rehamna massif of the Western Meseta in Morocco. The early Cambrian sample shows a single Paleoproterozoic population at ca. 2 Ga suggesting a local basement source. The Ordovician sample is largely dominated by a Cryogenian-Ediacaran population and minor Paleoproterozoic peaks. The Devonian sample reveals age populations similar to North-West African Cambrian to Devonian age spectra indicating that the southern-derived West Gondwana source essentially pertained up to the Devonian. The two early Carboniferous samples show more heterogeneous zircon age spectra with a marked Ediacaran peak

accompanied by Paleoproterozoic and Mesoproterozoic sub-peaks indicating important re-organization of the drainage systems. One sample also shows presence of Upper Devonian to early Carboniferous zircon grains, which suggests local magmatic sources associated to the formation of intracontinental extensional basins. The comparison of detrital zircon spectra with paleogeographic reconstructions indicate that the early Carboniferous change in detrital zircon sources can be interpreted in the framework of the opening of the Paleotethys ocean with coeval erosion of orogenic topographies linked to the emplacement of a Mid-Variscan Allochthon, and/or collision of an Avalonian indenter to the north.

Introduction

This paper presents a detrital zircon U–Pb geochronology study of samples from the Rehamna massif in the Moroccan Variscan belt (Michard *et al*., 2010), which aims at better constraining its lithostratigraphy and the evolution of source provenance during the Lower Paleozoic development. The hardness and resistance to chemical weathering make zircon one of the most durable minerals. Therefore, it can survive wide range of geological process (e.g. metamorphism, erosion and sedimentary transport) and preserve primary source signatures (Hanchar *and* Miller, 1993). In particular, detrital zircon grains in sedimentary rocks can survive multiple sedimentary cycles involving the recycling of old sedimentary, igneous and metamorphic rocks and younger primary crystalline sources (Thomas, 2011). Age distribution of detrital zircon in sedimentary rocks can be used for correlation of similar stratigraphic units, provenance analysis via comparison with known sources and determination of maximum depositional ages in the absence of datable contemporaneous volcanic rocks (Reiners *et al.*, 2017).

The paleogeographic evolution of the Moroccan Variscan belt (Fig. 1) is mostly based on geological mapping, tectonic studies and lithological correlations (Hoepffner *et al.*, 2005; Simancas *et al.*, 2005, 2009; Michard *et al.*, 2010; Chopin *et al.*, 2014). These ideas were

recently tested by a new generation of detrital zircon studies mostly used to precise paleogeography and source areas in northern Gondwana (e.g. Pereira *et al*., 2014; Perez-Caseres *et al.*, 2017; Letsch *et al.*, 2017; El Houicha *et al.*, 2018; Ghienne *et al.*, 2018; Perez *et al*., 2019; Accotto *et al.*, 2019, 2020, 2021a,b, 2022 and references therein). So far examined detrital zircon populations concern sedimentary rocks deposited in various late Neoproterozoic to Paleozoic basins preserved in the Moroccan Meseta. Their origin generally refers to recycling of the West African Craton (Archean domains, Eburnean Orogeny), the Pan-African Trans-Saharan belt, the Saharan Metacraton to the east, and their overlying Paleozoic strata (e.g., Accotto *et al*., 2019). Some studies focused on complete stratigraphic sections allow evaluating evolution of source areas through time or possible impact of remote geodynamic processes (e.g. Gärtner *et al.*, 2017; Accotto *et al.*, 2021). In this context, the Rehamna massif still remains understudied.

To fill the gap, a detrital zircon U–Pb geochronology study of a deformed Paleozoic sequence was performed in the southern part of the Rehamna massif of the Moroccan Meseta (Fig. 1). The present study aims at determining maximum depositional age of the strata and to give new insights into sedimentary provenance in an area where structural and stratigraphic uncertainties persist to date. Finally, this study allows to contribute to better understand the tectonic evolution of the northern Gondwana during late Paleozoic times.

Geological setting

The Paleozoic evolution of the Moroccan Variscan belt (Fig. 1) is well integrated in the evolution of the northern margin of Gondwana from its early Paleozoic extensional basins until its amalgamation with Laurussia during the late Carboniferous-early Permian (Michard *et al*., 2010; Chopin *et al.*, 2014; Martínez Catalán *et al.*, 2021). Three main Paleozoic events can be distinguished: (1) Since the late Cambrian formation of the Rheic ocean, the northern edge of the West African Craton (WAC) evolved in a passive margin environment (Stampfli *and* Borel,

2002; Ribeiro *et al.*, 2007; Oriolo *et al*., 2021). Avigad *et al*., (2012) showed that until the late Devonian, the sedimentation reflects the decreasing contribution of detrital material derived from local sources. (2) Subsequent formation of the Paleotethys ocean was associated to late Devonian-early Carboniferous intracontinental rifting (Stampfli *and* Borel, 2002; Frizon de Lamotte *et al.*, 2013). (3) This event was followed by the late Carboniferous-early Permian intracontinental Variscan Orogeny triggered by the collision between Gondwana with the European Variscan belt and Laurussia, which ultimately lead to the formation of Pangea (Hoepffner *et al*., 2005; Michard *et al.*, 2010; Chopin *et al*., 2014).

The Moroccan Meseta shows rare Precambrian basement units (e.g. Pereira *et al.*, 2015; El Houicha *et al*., 2018) unconformably overlain by thick Paleozoic successions deformed during the late Paleozoic (Michard *et al*., 2010; Chopin *et al*., 2014). The Variscan belt in Morocco can be divided into two main tectonic domains (Fig. 1; e.g., Piqué *et al.*, 1993a; Hoepffner *et al*., 2005; Michard *et al*., 2010): (1) the southern thick-skinned Anti-Atlas belt showing a fold and thrust belt with Paleozoic cover variably detached from its Precambrian basement, and (2) the Moroccan Meseta domain to the north of the Southern Meseta Fault (SMF) subdivided into two main zones, the Eastern and Western Meseta. The Eastern Meseta (e.g. Middelt, Tazekka, Debdou-Mekkam massifs) is characterized by deformed pre-Carboniferous sediments unconformably overlain by middle Visean to Serpukhovian-Bashkirian deposits (Hoepffner, 1987; Accotto *et al*., 2019, 2020). The Western Meseta (Michard *et al.*, 2010) consists of almost undeformed Cambrian-Devonian strata of its western "Coastal Block" and a central highly deformed and metamorphosed zone composed of crystalline basement covered by Cambrian-Carboniferous strata (Chopin *et al.*, 2014; Delchini *et al.*, 2018) outcropping in the Western High Atlas, Jebilet, Rehamna and Central massifs. The exotic Sehoul Block is located to the northwest and is either assumed to have an Avalonia (El Hassani, 1991; Piqué *et al*., 1993b; Tahiri *et al.*, 2010) or Meguma affinity (Michard *et al.*,

2010) and was accreted to the Moroccan Meseta during the early Carboniferous (Tahiri *et al.*, 2010).

Geology of the Rehamna massif

The Paleozoic Rehamna massif is situated midway south of Casablanca and north of Marrakech in the Western Meseta (Fig. 1). Its southern part is sometimes called the Rehamna metamorphic dome in contrast to the northern part (not shown in Fig. 2), which reveals solely the presence of comprehensive Cambrian to Permian sedimentary sequences. In this work we deal exclusively with the metamorphic southern part, which is also characterized by Precambrian inliers. The Rehamna massif is traditionally divided into three Western, Central and Eastern Rehamna zones separated by the Western Meseta Shear Zone (WMSZ, Fig. 1) or Median Fault and the Ouled Zednes Fault (Fig. 2; Michard *et al*., 2010; Chopin *et al*., 2014). Based on the intensity of deformation and the degree of metamorphism, the southern part is further subdivided into upper and lower metamorphic units (Fig. 3) according to the intensity of deformation and the degree of metamorphism (Baudin *et al*., 2003; Razin *et al.*, 2003; Michard *et al*., 2010; Chopin *et al*., 2014).

Lithostratigraphy

In contrast to the northern part of the Rehamna massif, where the age of the temporal framework of the succession is well understood (e.g. Hollard *et al*., 1982; El Kamel, 2002), the lithostratigraphy of its southern part is still controversial (Fig. 3; Destombes *et al.*, 1982; Baudin *et al.*, 2003; Razin *et al.*, 2003; Michard *et al.*, 2010). In the lower metamorphic units of the Central and Eastern Rehamna, the amphibolite facies metamorphism obliterated fossiliferous records, and the tentative stratigraphy is solely based on facies analogies with fossiliferous sedimentary sequences cropping out to the north (Hoepffner, 1974; Jenny, 1974).

The Paleoproterozoic basement of the Western Rehamna is characterized by metamorphosed porphyroids and rhyolites (Pereira *et al.*, 2015) covered by low-grade early-

middle Cambrian sediments (Fig. 3; Corsini *et al.,* 1988). The sequence starts with early Cambrian arkoses and limestones showing a gradually increasing detrital component (e.g. Lalla Mouchaa Formation; El Houicha *et al.,* 2018). This formation is conformably overlain by the "Paradoxides Shale Formation" composed of siltstone, greywacke and sandstone preserving a middle Cambrian fauna (Guézou *and* Michard, 1976; Corsini *et al*., 1988).

To the east of the WMSZ, a similar succession is present in the lower metamorphic unit of the Central Rehamna. Here, an early Ediacaran (593±8 Ma; Baudin *et al*., 2003) rhyolitic basement crops out in the core of the Sidi Ali dome (Fig.2; Corsini *et al*., 1988) and is conformably overlain by early Cambrian terrigenous clastic sediments (conglomerate, displaying granite and quartzite pebbles, interbedded with arkosic sandstone and mudstone; Fig. 3). A limestone sequence (including calcschists interbeds) marks the transition to early Cambrian siliciclastic sedimentation (Corsini *et al.,* 1988). The succession continues with early-middle Cambrian metapelitic strata (Draa El Kebir Formation) unconformably overlain by the Kef El Mouneb metaconglomerate assumingly Devonian (e.g. Hoepffner *et al.,* 1972). The age of the quartzites from the Skhour Formation of the upper metamorphic allochthonous unit is still controversial and was considered to be Ordovician by Destombes *et al.* (1982). However, based on structural and sedimentological arguments, Baudin *et al*. (2003) and Michard *et al*. (2010) alternatively proposed a possible Upper Devonian age for this formation (Fig. 3). The structurally lower metamorphic unit of the Eastern Rehamna is divided into the Devonian (Ouled Hassine-Ouled Zednes, OH-OZ) and Carboniferous (Lalla Tittaf) formations (Fig. 3). The former formation corresponds to a succession of pelitic beds interbedded with poorly-preserved Crinoidea-bearing limestones (Baudin *et al.,* 2003) and limy/sandy conglomerates or quartzites, generally attributed to the Devonian (Hoepffner, 1974). Preserved Eifelian-Frasnian corals were recently reported from this formation (marble of the Ouled Zednes area; El Houicha *et al.,* 2019). The Lala Tittaf Formation consists of pelites intercalated with andesites, gabbros

149 and rhyolites (Hoepffner, 1974; Cornée, 1982). Considered first as Carboniferous, Baudin *et al.*
150 (2003) proposed a Paleoproterozoic age based on the dating of zircon grains from a gabbroic
151 intrusion (2136 ± 17 Ma). However, this was challenged by a new U–Pb zircon data which
152 provide early Carboniferous ages (339.5 ± 0.89 Ma) for the intraformational rhyolite sills (Aït
153 Lahna *et al.*, 2018).

154 The upper unit to the north is formed by the allochthonous and very low grade Jbel
155 Kharrou and Koudiat El Adam Formations (Fig. 2) which are made of Middle Ordovician to
156 Silurian shale and sandstone (Destombes *et al.*, 1982). To the southeast and south of the Ouled
157 Ouggad Fault, the upper unit is represented by various virtually unmetamorphosed rocks (Fig.
158 2). The latter are composed of Ordovician strata overlain by Devonian (-Tournaisian?)
159 sandstone and pelite and by the middle (?) late Visean to Serpukhovian sandstone and limestone
160 including a sandy flysch facies typifying in the Dalaat unit (Fig. 3; Cornée, 1982; Razin *et al.*,
161 2003).

162 **Magmatism and metamorphism**

163 Two main metamorphic events were described in the southern part of the Rehamna massif. The
164 first one corresponds to a prograde Barrovian metamorphism (D1-M1) reaching the staurolite
165 (kyanite) stability field with estimated peak P-T at conditions 6–9 kbar and 410–560 °C. This
166 metamorphism affects the lower metamorphic unit during the late Carboniferous-early Permian
167 and was interpreted as a result of tectonic burial (Hoepffner *et al.*, 1982; Aghzer and Arenas,
168 1995; El Mahi et al., 1999; Chopin *et al*., 2014; Wernert *et al.*, 2016). The D1-M1 event was
169 followed by a greenschist facies retrograde metamorphism and D2 upright E-W folding of the
170 entire sequence (Chopin *et al*., 2014). This late tectonic event was probably contemporaneous
171 with the intrusion of the Ras El Abiod granitoid (Baudin *et al*., 2003). The M1 Barrovian and
172 M2 retrograde metamorphic events were dated at 310–295 Ma and 295–285 Ma, respectively
173 using $^{40}Ar/^{39}Ar$ (micas, amphiboles) and U–Pb (monazite) techniques (Chopin *et al*., 2014;

Wernert *et al*., 2016). Late to Post orogenic felsic magmatism (Piqué, 1979; Lagarde *et al*., 1989) is represented by the intrusions of the Sebt Brikiyine granite (Fig. 2) dated at ca. 275 Ma (e.g. Chopin *et al.,* 2014 and reference therein).

Methods - zircon separation, imaging and measurements

Two to four kilograms of rock per sample were processed at the laboratories of Czech Geological Survey in Prague. The zircon grains were separated by sieving (0.2 and 0.1 mm), heavy liquid (acetylene tetrabromide and methylene iodide) and magnetic separation. Then, they were selected randomly from the zircon concentrates by hand-picking under binocular microscope. The grains were mounted in epoxy discs, ground and polished. Cathodoluminescence (CL) and secondary electrons imaging were performed at the SEM Laboratory of the Czech Geological Survey (FEG-SEM TESCAN MIRA3 GMU working at 15 kV and ~22 mm working distance) in order to visualize internal zircon texture and zoning patterns of individual grains. We tried to get around 150 analyzes per sample which allowed to obtain representative and statistically significant age populations after discordant analyses are removed (Vermeesch, 2004).

The U–Pb dating of zircon grains was performed at the laboratories of the Czech Geological Survey. Measurements were performed on an Analyte Excite 193 nm excimer laser-ablation system (LA; Photon Machines), equipped with a two-volume HelEx ablation cell, in tandem with an Agilent 7900x ICPMS (Agilent Technologies Inc., Santa Clara, USA). Samples were ablated in He atmosphere (0.8 l min^{-1}) at a pulse repetition rate of 10 Hz using a spot size of 25 μm and laser fluence of 4.71 Jcm^{-2}. Each measurement consisted of 20 seconds of blank acquisition followed by ablation of the sample for a further 40 seconds of signal collection at masses 202, 204, 206, 207, 208, 232 and 238 using the SEM detector, with one point per mass peak and the respective dwell times of 10, 10, 15, 30, 20, 10 and 15 milliseconds per mass (total sweep time of 0.134 seconds). Instrumental drift was monitored by repeated measurements of

199 the 91500 (ca. 1063 Ma, Wiedenbeck *et al.,* 1995) reference zircon. Data deconvolution using
200 Iolite software followed the method described by Paton *et al.* (2010), including an 'on peak'
201 gas blank subtraction followed by correction for laser-induced elemental fractionation (LIEF)
202 by comparison with the behaviours of the 91500 reference zircon (Wiedenbeck *et al.,* 1995)
203 which yielded a concordia age at 1062.6 ± 1.6 Ma. No common Pb correction was applied in
204 this study. In addition, zircon reference samples GJ-1 (~609 Ma; Jackson *et al.,* 2004) and
205 Plešovice (~337 Ma; Sláma *et al.,* 2008) were analysed periodically during this study and
206 yielded concordia ages at 609.3 ±1.5 Ma and 338.5 ±1.0 Ma (2σ), respectively.
207 The analytical data were plotted using the IsoplotR toolbox (Vermeesch, 2018). Data
208 reduction followed the recommendation of Spencer *et al.* (2016) whereby data is treated as
209 concordant if the 2σ ellipse overlaps with the concordia, and the preferred ages are single zircon
210 concordia ages following the recommendations of Nemchin and Cawood (2005) and
211 Zimmermann *et al.* (2018). For all concordant ages younger than 1000 Ma the $^{206}Pb/^{238}U$ ages
212 were used, whereas older ages are based on the obtained $^{207}Pb/^{206}Pb$ ratios (Gehrels, 2012). We
213 kept U–Pb zircon ages with a degree of concordance situated in between 95% and 105% which
214 corresponds to the number of analyzed zircon needed to get sufficient representative data.

215 ## 4.Results

216 In this study, we collected early Cambrian to Mississippian (meta)sandstone samples from eight
217 sites for U–Pb detrital zircon geochronology. From each location, we took several pieces of
218 rock from the main sedimentary strata to ensure the representativeness of the sampling. The
219 geographic, geological and stratigraphic characteristics of each sampling sites are shown in
220 figures 2 and 3, and table 1. Note that no zircon grain were found after mineral separation of
221 (meta)clastic rocks samples from the Draa El Kebir, Kef El Mouneb and Lalla Tittaf
222 Formations. Therefore, only five age spectra are presented in the following.

Sample R16-1A

The sample R16-1A was collected at the southern border of the Sebt Brikiyine granitic intrusion (Fig. 2). It is an early Cambrian arkosic metasandstone overlying the Paleoproterozoic basement (Pereira *et al*., 2015) with an essentially preserved unconformable stratigraphic contact, which was, however, possibly tectonically reactivated (Fig. 3, Fig. 4a). This deformed arkosic metasandstone (Fig. 4b) is composed of equigranular fine-grained quartz grains with well equilibrated straight boundaries ranging from 60 to 500 µm in size. Feldspar and muscovite grains show incipient recrystallization (Fig. 5a). Polygonal zircon grains with angular shape are 120–200 µm grains size while sub-rounded grains of irregular shape are smaller (<50 µm). Most of zircon grains show homogeneous cores surrounded by a brighter oscillatory domain (CL-light) and darker rim (CL-dark; Fig. 6a). The grains are commonly fractured. One hundred seventeen concordant ages from 230 analyses were obtained (Fig. 7a), showing a unimodal Paleoproterozoic age spectrum (Fig. 7b) peaking at ca. 2000–2100 Ma (mean age 2048.3 ± 1.4 Ma).

Sample SK1-Z

The sample SK1-Z was collected from a quartzitic level surrounded by low grade schist of the Ordovician-Devonian (?) Skhour Formation (Fig. 2, Fig. 3, Fig. 4c). This highly deformed quartzite is characterized by well equilibrated quartz foam texture with subequant quartz grains 150–200 µm in size with straight boundaries and an excellent triple point network. (Fig. 5b). The zircon population consists of elongated, sub-euhedral to euhedral grains 140–180 µm in size and few more rounded smaller grains 60–100 µm in size. The analyzed zircon grains are characterized by a prismatic and sector zoning with some fractures and inclusions (Fig. 6b). Ninety-four concordant ages from 123 analyses were obtained (Fig. 8a). Cryogenian-Ediacaran ages (540–850 Ma) constitutes 73% of all analyses with a peak at ca. 626 Ma. There are very

subordinate clusters at 1700–2200 Ma (18%) and another one at ca. 1 Ga (1%). A small peak at ca. 580 Ma is also present (Fig. 8a).

Sample R257-OH

R257-OH was collected in quartzite lenses of the eastern extremity of the OH-OZ Formation (near the Souk el Had; Fig. 2, Fig. 3). The formation can be either Lower or Middle to Upper Devonian (El Houicha *et al.*, 2019) depending on the interpretation of the stratigraphic polarity (e.g. Hoepffner, 1974; Cornée, 1982; Razin *et al.*, 2003). These weakly metamorphosed and deformed impure quartzite (Fig. 4d) is composed of recrystallized, elongate grains of quartz with lobate boundaries and irregular undulatory extinction and minor recrystallized muscovite (Fig. 5c). Large detrital zircon grains (100–150 µm) have a long prismatic shape whereas smaller zircon population (50–75 µm in size) are sub-rounded. Most of the large zircons show a sector zoning but some are characterized by prismatic zonation patterns (Fig. 6c). Several rounded grains are homogeneous and weakly luminescent. A set of 138 concordant ages has been obtained from 161 analyses (Fig. 8a). They show a main Cryogenian-Ediacaran population (540–850 Ma; 79%) with a peak at ca. 632 Ma and a smaller Paleoproterozoic cluster (1700–2200 Ma; 17%) with two peaks at ca. 1764 and 2071 Ma. Distributed Mesoproterozoic and Archean ages are also present (Fig. 8b).

Sample R255-OZ

The sample R255-OZ was collected next to the fossiliferous Eifelian-Frasnian limestones (El Houicha *et al.*, 2019) of the OH-OZ Formation along the Ouled-Zednes Fault zone (Fig. 2, Fig. 3). The site shows a narrow belt of steeply SE-dipping quartzite, shale and limestone of the OH-OZ Formation surrounded by Skhour Formation rocks in the northwest and Koudiat El Adam rocks in the SE (Fig. 4g,e). The sampled rock is a light-grey low-grade quartzite (Fig. 4f) showing incipient bulging type recrystallization at margins of detrital quartz grains (100 to 200 µm in size) and presence of small sericite grains (Fig. 5d). The age of this rock is probably

Upper Devonian (post-Frasnian) to Dinantian in stratigraphic continuity with the Middle Devonian Ouled Zednes Formation of the lower metamorphic unit (Jenny, 1974; Razin, 2003; Baudin et al., 2003). However, Baudin *et al.* (2003) did not exclude that it might represent a tectonic slice from the upper metamorphic unit, either from the western Cambro-Ordovician or Upper Devonian Skhour Formation, or from the eastern Ordovician Jbel Kharrou-Koudiat El Adam nappe (Fig. 2). The zircon grains reveal a complex texture in their CL images with variable luminescence and patterns. Most of the extracted detrital zircon from this sample is about 60–100 µm in size, showing oscillatory or sector zoned with irregular or straight grain boundaries. Less frequently, low- to high luminescent homogenous elongated grains 120–140 µm in size are present (Fig. 6d). One hundred twenty-two concordant ages from 178 analyses have been obtained from this sample (Fig. 8c). They show multimodal age spectra ranging between 310–540 Ma (13%), 540–850 Ma (52%), 850–1200 Ma (15%) and 1500–2200 Ma (15%). A younger population shows subordinate peaks at 477 and 559 Ma. Nevertheless, the youngest detrital zircon ages are close to 350 Ma (Fig. 6d, Fig. 8c).

Sample R256-DT

The sample R256-DT was collected from the Dalaat unit (member 2 in the Dalaat Formation s.s.; Razin *et al.*, 2003; Fig. 2; Fig. 3). This unit corresponds to middle (?)-late Visean basal fine to medium grained arkosic sandstones alternating with limestone (Fig. 4h,i). The sandstone is composed of quartz and feldspar grains, 150–400 µm in size, some detrital muscovite, chloritized biotite and interstitial calcite (Fig. 5e). The zircon grains show either subhedral shapes and oscillatory and sector zoning or sub-rounded shapes and homogeneous weakly or highly luminescent patterns (Fig. 6e). The studied zircon grain size falls primarily into the 120–170 µm range and less frequently into the 60–100 µm range. A total of 182 analyses were carried out, of which 136 displayed concordant ages (Fig. 8d). The sample R256-DT is dominated by a Cryogenian-Ediacaran population (68%) ranging between 540 and 850 Ma with

297 a peak at 633.9 ± 0.5 Ma and three subordinate populations at 850–1200 Ma (12%), 1500–2200
298 Ma (13%) and 2200–2500 Ma (13%) suggesting potential peaks around 991 Ma, 1943 Ma and
299 2446 Ma, respectively (Fig. 8b).

300 Most of the analyses from all the samples are characterized by Th/U ratios > 0.1 (ranging
301 between 0.1 and 1.7) suggesting a primary magmatic origin (Rubatto, 2002). However, some
302 zircon rims show Th/U ratios lower than 0.1, in particular those in the 600–850 Ma range, which
303 is compatible with a metamorphic remobilization.

304 # 5. Discussion

305 ## Evolution of detrital zircon sources in time

306 South of the Sebt Brikiyine granite, Pereira *et al.* (2015) described an Eburnean basement dated
307 at 2050.6 ± 3.0 Ma (SHRIMP U–Th–Pb, rhyolitic porphyry, sample SBR-21 in Fig. 2 and Fig.
308 3). The basement is unconformably overlain by clastic (pelites, arkoses) and carbonate
309 (limestones and calcschists) strata similar to the early Cambrian succession outcropping in the
310 northern Lalla Mouchaa Formation and in the Sidi Ali dome in the lower metamorphic unit of
311 the Central Rehamna (Corsini *et al.*, 1988). The sample R16-1A (Fig. 2), an arkosic sandstone
312 directly overlying the Paleoproterozoic basement, only show zircon grains with
313 Paleoproterozoic ages (mean age 2048.3 ± 1.4 Ma). This cluster is similar to the one obtained
314 from early Cambrian microbreccia from the Lalla Mouchaa Formation (Sample NB1; Fig. 2,
315 Fig. 3) with detrital zircons at ca. 2047 ± 12 Ma (El Houicha *et al*., 2018). Both samples (R16-
316 1A, this study, and NB1, El Houicha *et al.*, 2018) are characterized by angular feldspar and
317 euhedral zircons, the latter with concentric zoning suggesting a magmatic origin and a low
318 roundness indicative for a very short transport distance and thus, low-order recycling of
319 sediments. Correlation with published ages shows that the detrital zircon likely derived from
320 first-cycle erosion of the local Eburnean basement (Pereira *et al.*, 2015) indicating proximal

watersheds collecting the signal from the nearby rocks (Fig. 9a). At regional scale, the detrital zircons from the basal early Cambrian sediments overlying the Meseta basement reflect exclusive, local recycling of the heterogeneous Precambrian basement. Indeed, detrital zircons ages from the early Cambrian microbreccia at Lalla Mouchaa and (meta)arkose from south of Sebt Brikiyine granite are perfectly similar to the age of the underlying rhyolitic basement (2050.6 ± 3.0 Ma, sample SBR-21 in Pereira *et al.,* 2015). Similarly, a single Cadomian/Pan-African cluster is found in detrital zircon from the early Cambrian microbreccia (ca. 583, sample JD2) covering the El Jadida rhyolitic basement dated at 584.2 ± 4.8 Ma, sample JD-1 in El Houicha *et al.*, 2018). Finally, the Neoproterozoic metavolcanic rocks from the Sidi Ali Dome (593 ± 8 Ma, Baudin et al., 2003) is covered by early Cambrian metaconglomerates containing granitic pebbles showing zircon ages in the range 600–640 Ma (Pereira *et al.* (2014), whereas detrital zircons ages from the matrix are in the range 548–624 Ma (Sample 15DL11 in Letsch *et al.,* 2018). This discrimination between Eburnean and Cadomian/Pan-African basements and sources in the Western Meseta, might reflect an inherited suture zone originating the WMSZ since the early Paleozoic (e.g. Piqué et al., 1980, Corsini, 1991).

Samples SK1-Z (upper metamorphic unit) and R257-OH (lower metamorphic unit) show very similar density probability curves, largely dominated by a Cryogenian-Ediacaran population, including a late Ediacaran subpopulation. Additionally, there is a Paleoproterozoic population ranging between 1700–2200 Ma. The main Pan-African peak with moderate Paleoproterozoic ages is typical of West African Cambrian to Devonian age spectra (Gärtner *et al.*, 2017; Letsch *et al.,* 2018; Ghienne *et al.*, 2018; Accotto *et al.,* 2021b). Similar age populations might indicate that those two samples originally belong to the same stratigraphic unit: the Devonian stratigraphic age of the R257-OH sample (Fig. 2, Fig. 3) might therefore suggest that the SK1-Z sample is also from a Devonian unit, as proposed by Baudin *et al.* (2003) and Michard *et al.* (2010). However, detrital zircon data from the Central massif (Accotto *et*

346 *al.*, 2021b) show that such an age spectrum does not allow differentiating Ordovician from
347 Devonian strata and that similar zircon populations are identified in both the Ordovician of
348 some of the autochthonous strata (Ezzhelligha area, EZ on the Fig. 1) and allochthonous strata
349 (Azrou area, AZR on the Fig. 1). Nevertheless, because sample SK1-Z has affinities with both
350 Ordovician samples from the Ezzhelligha area (Accotto *et al.*, 2021b) and the late Cambrian
351 (El Hank) from the nearby Coastal Block (sample 15DL12, IMF on the Fig. 1) (Letsch *et al.*,
352 2018), we favor an Ordovician age for the SK1-Z rock unit, and not favor an Upper Devonian
353 age as suggested by Baudin *et al.* (2003) and Michard *et al.* (2010). Whatever the stratigraphic
354 attribution of the samples might be, SK1-Z and R257-OH and similar ones from the Meseta
355 show that the southern-derived West Gondwana source (i.e. dominant Cadomian/Pan-African
356 and Eburnean source) essentially pertained from the Cambrian-Ordovician up to the Devonian
357 (Fig. 9b; Gärtner *et al.*, 2017; Accotto *et al.*, 2021b). The minor presence of Meseoproterozoic
358 zircons, also described elsewhere in the Meseta might reflect a minor lateral source from the
359 Sahara Metacraton (see however discussion in Accotto et al., 2021b).

360 The sample R255-OZ collected in the OH-OZ Formation shows a major change with two
361 grains indicating a maximum depositional age as young as early Carboniferous (350.6 ±10 Ma
362 and 352.5 ±7 Ma, i.e Tournaisian), i.e. significantly younger than the Devonian strata hosting
363 the sample R257-OH. This is in full agreement with a distinctive age spectrum, showing
364 Ordovician to Lower Devonian subordinate peaks and a less prominent Pan-African population.
365 As in R256-DT (see next paragraph), Mesoproterozoic zircon grains are present but more
366 distributed within the Mesoproterozoic instead of a peak at ~1 Ga. It suggests a different
367 sourcing, confirmed by the morphology of zircons which are mostly euhedral and poorly
368 rounded —in contrast to detrital zircons from the underlying Cambrian to Devonian strata—,
369 indicating a relatively short transportation path. If the Cambrian to Lower Ordovician zircon
370 grains can be derived from nearby sedimentary sources (Letsch *et al.*, 2018; Accotto *et al.*,

2021b), again indicating the recycling of the Meseta early Paleozoic sedimentary cover, occurrences of late Paleozoic and Mesoproterozoic zircon grains suggests in addition great changes in the distribution of the watersheds. In particular, the latter are well known to include renewed volcanic activity at the regional scale (Kharbouch, 1994; Moreno *et al.*, 2008; Aït Lahna *et al.*, 2018). The source of Mesoproterozoic zircons might reflect the presence of an allochthonous unit positioned to the north and docked in the course of the Variscan collision as suggested from studies in the Eastern Meseta (e.g. Accotto *et al.*, 2020b). However, the limited number of "Variscan" late Paleozoic zircons grains in the Rehamna massif, which are largely more represented in the Eastern Meseta, makes this sourcing from the northern watersheds unlikely. On the other hand, the sediment transport scenario from the WAC cannot be excluded. The samples R255-OZ and R256-DT show some increased Mesoproterozoic component which is well known from the sedimentary cover of the western edge of the WAC (Taoudeni basin; Bradley *et al.*, 2015; Gärtner et al., 2017). Moreover, detrital zircon data indicates a dispersal of Mesoproterozoic detritus since Cambrian times (e.g. Gärtner *et al.*, 2017; Fig 10b). Derivations from either the southwest, running parallel to the continental margin and the coevally forming orogen, or from the northwest (Avalonia or European Variscan Orogen; i.e., orthogonal to the Variscan collision) might be postulated.

The middle (?)-late Visean sample R256-DT collected from the basal siliciclastic Dalaat Formation is also dominated by Ediacaran to Cryogenian ages but with other subordinate, yet significant signals: distributed Mesoproterozoic zircon grains, a small but definite Stenian-Tonian peak, and a early Cryogenian subpopulation. It may be interpreted as a continuum of the Cambrian-Ordovician source, with addition of subordinate new sources, or, alternatively, as the recycling of Meseta-derived Cambrian-Devonian strata (Fig. 9d) because all of the additional signals are also present, admittedly in various proportion, in Lower Paleozoic strata outcropping in the Meseta, and more specifically in northern and north-eastern Meseta

(Ghienne *et al.,* 2018; Accotto *et al.,* 2020a; 2021). A combination of the two schemes, a western Gondwana source combined with the recycling of older strata, is in fact likely.

Geodynamic implications

This study indicates a modification through time of detrital sources feeding the continental shelf and the sedimentary basins in the current Rehamna area, which is compatible with the geodynamic model recently proposed for the Variscan belt (Martínez Catalán *et al.,* 2021). The reconstructions based on existing paleomagnetic and geological data and models of Domeier and Torsvik (2014) and Matthews *et al.* (2016) allow to visualize evolution of zircon sources as suggested in this work, in complementing and agreeing with the study of Accotto *et al.* (2021a). Since the Ordovician, the northern Gondwana has evolved in a passive margin setting, suggesting that the detrital zircon populations deposited in Ordovician to Lower Devonian basins were entirely governed by recycling Gondwanan sources from the south and SE, represented either by remote exposed basements, and/or their sedimentary covers (Fig. 10a). However, the situation radically changed owing to two separate late Devonian to early Carboniferous events. The first one is related to the propagation of the Paleotethys ocean (Stampfli et al., 2003; Stampfli et al., 2013) into the interior of Gondwana thereby forming the network of basins typical for Eastern and Western Meseta (Cózar *et al.,* 2020) and oceanic realm further east (Edel *et al.,* 2018; Fig. 10b), which is typified in the Rehamna massif by the formation of the Devonian to early Carboniferous basins and associated magmatism (Hoepffner, 1974; 1982; Aït Lahna *et al.,* 2018). At the same time, a ribbon fragment of Gondwana called the Mid-Variscan Autochthon was obducted by giant allochthonous nappe complexes (Martínez Catalán *et al.,* 2021) involving both oceanic and continental rocks (Fig. 10b). This event occurred simultaneously with possible westward indentation of Avalonian promontory with the Variscan autochthon as discussed by Accotto *et al.* (2021a). It was recently shown that the Mid-Variscan allochthon also contains sedimentary sequences with abundant

Mesoproterozoic zircon signature (Lindner *et al.*, 2021) previously considered as typical for Avalonia (Mazur *et al.*, 2010).

Therefore, the opening of Lower Devonian to Carboniferous sedimentary basins within the Moroccan Meseta was coeval with a major convergent event in the north. In this context, Mesoproterozoic zircons grains of the late Paleozoic Rehamna record are thought to have principally originated from the convergent deformation zone, derived from either an Avalonian (e.g. Gärtner *et al.*, 2018) or mid-Allochthonous (e.g. Lindner *et al.*, 2021) source, even though the massive peak at 1.3 Ga from the latter could be "diluted" in our samples. Indeed, a contribution through recycling of the sedimentary cover of the WAC cannot be totally excluded. Anyway, the source of Mesoproterozoic zircons from the Variscan core and/or Avalonian indenter (Accotto *et al.*, 2021a) remain questionable as the early Carboniferous paleo-geographic position of both possible source areas remains poorly constrained. To the contrary, early Carboniferous zircon grains (sample R255-OZ) are argued to principally derived from early Carboniferous magmatism reported in the Moroccan Meseta (Kharbouch, 1994), although we note that the Mid-Variscan Allochthon was intruded by series of magmatic arcs from 380 to 350 Ma (e.g. Lardeaux *et al.*, 2014; Deiller *et al.*, 2021) which could have also contributed to the detrital zircon record in the Rehamna basin.

Acknowledgments

The authors want to gratefully acknowledge Nikol Novotná (SEM laboratory) and the technician from the Czech Geological Survey involved in the preparation of the samples. This work was supported by the TelluS Program of CNRS/INSU and institutional grants from the Czech Geological Survey (grant number 310270 and DKRVO) and from the CNRS IPGS UMR7516 (now ITES UMR 7063). The University Chouaïb Doukkali and Martin Simon are thanked for their support during the field work. Fabien Humbert (Southern University of Science and Technology, Shenzhen) is thanked for the processing of photographs.

References

Accotto, C., Martínez Poyatos, D.J., Azor, A., Talavera, C., Evans, N.J., Jabaloy-Sánchez, A., Azdimousa, A., Tahiri, A., El Hadi, H., 2019. Mixed and recycled detrital zircons in the Paleozoic rocks of the Eastern Moroccan Meseta: Paleogeographic inferences. Lithos, 338–339, 73–86. https://doi.org/10.1016/j.lithos.2019.04.011

Accotto, C., Martínez Poyatos, D., Azor, A., Jabaloy-Sánchez, A., Talavera, C., Evans, N.J., Azdimousa, A., 2020. Tectonic Evolution of the Eastern Moroccan Meseta: From Late Devonian Forearc Sedimentation to Early Carboniferous Collision of an Avalonian Promontory. Tectonics, 39, 1–29. https://doi.org/10.1029/2019TC005976

Accotto, C., Martínez Poyatos, D., Azor, A., Talavera, C., Evans, N.J., Jabaloy-Sánchez, A., Azdimousa, A., Tahiri, A., El Hadi, H., 2021a. Syn-collisional detrital zircon source evolution in the northern Moroccan Variscides. Gondwana Research, 93, 73–88. https://doi.org/10.1016/j.gr.2021.02.001

Accotto, C., Martínez Poyatos, D., Azor, A., Talavera, C., Evans, N.J., Jabaloy–Sánchez, A., Tahiri, A., El Hadi, H., Azdimousa, A., 2021b. Systematics of detrital zircon U–Pb ages from Cambrian–Lower Devonian rocks of northern Morocco with implications for the northern Gondwanan passive margin. Precambrian Research, 365. https://doi.org/10.1016/j.precamres.2021.106366

Accotto, C., Martínez Poyatos, D., Azor, A., Talavera, C., Evans, N.J., Jabaloy-Sánchez, A., El Hadi, H., Tahiri, A., 2022. Detrital zircon sources in the Ordovician metasedimentary rocks of the Moroccan Meseta: Inferences for northern Gondwanan passive-margin paleogeography, in: New Developments in the Appalachian-Caledonian- Variscan Orogen. Geological Society of America. https://doi.org/10.1130/2021.2554(17)

Aghzer, A.M., Arenas, R., 1995. Détachements et tectonique extensive dans le massif hercynien des Rehamna (Maroc). Journal of African Earth Sciences, 21, 383–393. https://doi.org/10.1016/0899-5362(95)00096-C

Aït Lahna, A., Aarab, E.M., Nasrrddine, Y., Colombo Celso Gaeata, T., Bensalah, M., Boumehdi, M.A., Kei, S., Basei, M.A.S., 2018. The Lalla Tittaf Formation (Rehamna, Morocco): Paleoproterozoic or Paleozoic age?, in: ICG2018-Joint Congress-CAAWG9-CAAWG9-ArabGU2-ICGAME3, Abstract Book. El Jadida, pp. 13–16.

Avigad, D., Gerdes, A., Morag, N., Bechstädt, T., 2012. Coupled U-Pb-Hf of detrital zircons of Cambrian sandstones from Morocco and Sardinia: Implications for provenance and Precambrian crustal evolution of North Africa. Gondwana Research, 21, 690–703. https://doi.org/10.1016/j.gr.2011.06.005

Baudin, T., Chévremont, P., Razin, P., Youbi, N., Andries, D., Hoepffner, C., Thiéblemont, D., Chihani, E., Tegyey, M., 2003. Carte géologique du Maroc au 1/50 000, feuille de Skhour des Rehamna, Mémoire explicatif. Notes et Mémoires du Service Géologique du Maroc, Rabat, 435 bis, 1–114.

Bradley D.C., O'Sullivan P., Cosca M.A., Motts H.A., Horton J.D., Taylor C.D., Beaudoin G., Lee GK., Ramezani J., Bradley DB., Jones JV., Bowring S., 2015. Synthesis of geological, structural, and geochronologic data (Phase V, Deliverable 53). Chapter A of Taylor CD (ed.), Second Projet de Renforcement Institutionnel du Secteur Minier de la République Islamique de Mauritanie (PRISM-II). U.S. Geological Survey Open-File Report 2013 12080-A, 328p. doi:10.3133/ofr20131280

Chopin, F., Corsini, M., Schulmann, K., El Houicha, M., Ghienne, J.-F., Edel, J.-B., 2014. Tectonic evolution of the Rehamna metamorphic dome (Morocco) in the context of the

493 Alleghanian-Variscan orogeny. Tectonics, 33, 1154–1177.
494 https://doi.org/10.1002/2014TC003539
495 Cornée, J.-J., 1982. Étude lithostratigraphique et tectonométamorphique des Rehamna sud-
496 orientales. Plissements et nappes. Contribution à la connaissance de la chaîne hercynienne
497 en Meseta marocaine. Trav. Lab. Sci. Terre, Saint Jérôme, Université Aix–Marseille III,
498 Aix-Marseille.
499 Corsini M., 1991. Influence de la paléogéographie du Paléozoïque sur les déformations
500 hercyniennes de la Meseta nord-occidentale du Maroc. Géologie Méditerranéenne, 18,
501 (1-2), 73–80. https://doi.org/10.3406/geolm.1991.1453
502 Corsini, M., Muller, J., Cornée, J.-J., Diot, H., 1988. Découverte de la série basale du Cambrien
503 et de son substratum dans les Rehamna centraux, haut-fond au Cambrien (Meseta
504 marocaine). Prémices de l'orogenèse hercynienne. Comptes Rendus de l'Académie des
505 sciences, Série II, 306, 63–68.
506 Cózar, P., Vachard, D., Izart, A., Said, I., Somerville, I., Rodríguez, S., Coronado, I., El
507 Houicha, M., Ouarhache, D., 2020. Lower-middle Viséan transgressive carbonates in
508 Morocco: Palaeobiogeographic insights. Journal of African Earth Sciences, 168.
509 https://doi.org/10.1016/j.jafrearsci.2020.103850
510 Deiller, P., Štípská, P., Ulrich, M., Schulmann, K., Collett, S., Peřestý, V., Hacker, B.,
511 Kylander-Clark, A., Whitechurch, H., Lexa, O., Pelt, E., Míková, J., 2021. Eclogite
512 subduction wedge intruded by arc-type magma: The earliest record of Variscan arc in the
513 Bohemian Massif. Gondwana Research, 99, 220–246.
514 https://doi.org/10.1016/J.GR.2021.07.005
515 Delchini, S., Lahfid, A., Lacroix, B., Baudin, T., Hoepffner, C., Guerrot, C., Lach, P., Saddiqi,
516 O., Ramboz, C., 2018. The Geological Evolution of the Variscan Jebilet Massif, Morocco,
517 Inferred From New Structural and Geochronological Analyses. Tectonics, 37, 4470–
518 4493. https://doi.org/10.1029/2018TC005002
519 Destombes, J., Guézou, J.-C., Hoepffner, C., Jenny, P., Piqué, A., Michard, A., 1982. Le
520 Primaire du massif des Rehamna s.s., problèmes de stratigraphie des séries
521 métamorphiques, in: Michard, A. (Ed.), Le massif Paléozoïque des Rehamna (Maroc):
522 Stratigraphie, Tectonique et Petrogenese d'un segment de la Chaine Varisque. Notes et
523 Mémoires du Service Géologique, Rabat 303, pp. 35–70.
524 Domeier, M., Torsvik, T.H., 2014. Plate tectonics in the late Paleozoic. Geoscience Frontiers,
525 5, 303–350. https://doi.org/10.1016/j.gsf.2014.01.002
526 Edel, J.-B., Schulmann, K., Lexa, O., Lardeaux, J.M., 2018. Late Palaeozoic palaeomagnetic
527 and tectonic constraints for amalgamation of Pangea supercontinent in the European
528 Variscan belt. Earth-Science Reviews, 177, 589–612.
529 https://doi.org/10.1016/j.earscirev.2017.12.007
530 El Hassani, A., 1991. La Zone de Rabat-Tiflet: bordure nord de la Chaîne Calédono-
531 Hercynienne du Maroc. Bulletin de l'Institut Scientifique, Rabat, 15, 1–34.
532 El Houicha, M., Aboussalam, Z.S., Rodriguez, S., Chopin, F., Jouhari, A., Schulmann, K.,
533 Ghienne, J-F., Becker, R.T., 2019. Discovery of Eifelian-Frasnian corals in metamorphic
534 rocks from the Rehamna massif (Moroccan Meseta): biostratigraphic and
535 paleogeographic implications. 11th Colloquium 3MA « Magmatism, Metamorphism and
536 associated Mineralization », 38–40.
537 El Houicha, M., Pereira, M.F., Jouhari, A., Gama, C., Ennih, N., Fekkak, A., Ezzouhairi, H., El
538 Attari, A., Silva, J.B., 2018. Recycling of the Proterozoic crystalline basement in the
539 Coastal Block (Moroccan Meseta): New insights for understanding the geodynamic
540 evolution of the northern peri-Gondwanan realm. Precambrian Research, 306, 129–154.
541 https://doi.org/10.1016/j.precamres.2017.12.039

El Kamel, F., 2002. Sédimentologie, magmatisme pré-orogénique et structuration du Paléozoïque des Rehamna et d'Ouled Abbou (Meseta occidentale, Maroc). Thèse, Doctorat ès-Sciences, Université Hassan II, Casablanca, Maroc, 208 p.

El Mahi, B., Hoepffner, C., Zahraoui, M., Boushaba, A., 1999. L'évolution structurale et métamorphique de la zone hercynienne des Rehamna centraux (Maroc). GAW 4, International Conference on Geology of the Arab World, Cairo University, Egypt, pp. 26–45.

Frizon de Lamotte, D., Tavakoli-Shirazi, S., Leturmy, P., Averbuch, O., Mouchot, N., Raulin, C., Leparmentier, F., Blanpied, C., Ringenbach, J.-C., 2013. Evidence for Late Devonian vertical movements and extensional deformation in northern Africa and Arabia: Integration in the geodynamics of the Devonian world. Tectonics, 32, 107–122. https://doi.org/10.1002/tect.20007

Gärtner, A., Villeneuve, M., Linnemann, U., El Archi, A., Bellon, H., 2013. An exotic terrane of Laurussian affinity in the Mauritanides and Souttoufides (Moroccan Sahara). Gondwana Research, 24, 687–699. https://doi.org/10.1016/j.gr.2012.12.019

Gärtner, A., Youbi, N., Villeneuve, M., Sagawe, A., Hofmann, M., Mahmoudi, A., Boumehdi, M.A., Linnemann, U., 2017. The zircon evidence of temporally changing sediment transport—the NW Gondwana margin during Cambrian to Devonian time (Aoucert and Smara areas, Moroccan Sahara). International Journal of Earth Sciences, 106, 2747–2769. https://doi.org/10.1007/s00531-017-1457-x

Gärtner, A., Youbi, N., Villeneuve, M., Linnemann, U., Sagawe, A., Hofmann, M., Zieger, J., Mahmoudi, A., Boumehdi, M.A., 2018. Provenance of detrital zircon from siliciclastic rocks of the Sebkha Gezmayet unit of the Adrar Souttouf Massif (Moroccan Sahara) – Palaeogeographic implications. Comptes Rendus Geoscience, 350, 255–266. https://doi.org/10.1016/j.crte.2018.06.004

Gehrels, G., 2012. Detrital Zircon U-Pb Geochronology: Current Methods and New Opportunities, in: Tectonics of Sedimentary Basins. John Wiley & Sons, Ltd, Chichester, UK, pp. 45–62. https://doi.org/10.1002/9781444347166.ch2

Ghienne, J.F., Benvenuti, A., El Houicha, M., Girard, F., Kali, E., Khoukhi, Y., Langbour, C., Magna, T., Míková, J., Moscariello, A., Schulmann, K., 2018. The impact of the end-Ordovician glaciation on sediment routing systems: A case study from the Meseta (northern Morocco). Gondwana Research, 63, 169–178. https://doi.org/10.1016/j.gr.2018.07.001

Guézou, J.-C., Michard, A., 1976. Note sur la structure du môle côtier mésétien dans l'ouest des Rehamna (Maroc hercynien). Sciences Géologiques, Bulletin, Strasbourg, 29, 171−182.

Hanchar, J.M., Miller, C.F., 1993. Zircon zonation patterns as revealed by cathodoluminescence and backscattered electron images: Implications for interpretation of complex crustal histories. Chemical Geology, 110, 1–13. https://doi.org/10.1016/0009-2541(93)90244-D

Hoepffner, C., 1974. Contribution à la géologie structurale des Rehamna (Meseta marocaine méridionale), le matériel paléozoïque et son évolution hercynienne dans l'est du massif. Thèse 3ème cycle, Université Louis Pasteur, Strasbourg, France.

Hoepffner, C., 1987. La tectonique hercynienne dans l'Est du Maroc. Thèse ès sciences, Université Louis Pasteur, Strasbourg, France.

Hoepffner, C., Jenny, P., Piqué, A., Michard, A., 1982. Le métamorphisme hercynien dans le massif des Rehamna, in: Michard, A. (Ed.), Le massif Paléozoïque des Rehamna (Maroc): Stratigraphie, Tectonique et Petrogenese d'un segment de la Chaine Varisque. Notes et Mémoires du Service Géologique, Rabat, 303, pp. 130–149.

Hoepffner, C., 1982. Le magmatisme pré- et post-orogénique hercynien dans le massif des Rehamna, in: Michard, A. (Ed.), Le massif Paléozoïque des Rehamna (Maroc): Stratigraphie, Tectonique et Petrogenese d'un segment de la Chaine Varisque. Notes et Mémoires du Service Géologique, Rabat, 303, pp. 150–163.

Hoepffner, C., Soulaimani, A., Piqué, A., 2005. The Moroccan Hercynides. Journal of African Earth Sciences, 43, 144–165. https://doi.org/10.1016/j.jafrearsci.2005.09.002

Hollard, H., Michard, A., Jenny, P., Hoepffner, C., Willefert, S., 1982. Stratigraphie du Primaire de Mechra-Ben-Abbou, Rehamna, in: Michard, A. (Ed.), Le massif Paléozoïque des Rehamna (Maroc): Stratigraphie, Tectonique et Petrogenese d'un segment de la Chaine Varisque. Notes et Mémoires du Service Géologique, Rabat, 303, pp. 12–34.

Jackson, S.E., Pearson, N.J., Griffin, W.L., Belousova, E.A., 2004. The application of laser ablation-inductively coupled plasma-mass spectrometry to in situ U-Pb zircon geochronology. Chemical Geology, 211, 47–69. https://doi.org/10.1016/j.chemgeo.2004.06.017

Jenny, P., 1974. Contribution à la géologie structurale des Rehamna (Meseta marocaine méridionale). Le matériel paléozoïque et son évolution hercynienne dans le centre du massif. Thèse 3ème cycle, Université Louis Pasteur, Strasbourg, France.

Kharbouch, F., 1994. Le volcanisme dévono-dinantien du Massif central et de la Meseta orientale. Bulletin de l'Institut Scientifique, Rabat, 18, 192–200.

Lagarde, J.-L., Ait Ayad, N., Ait Omar, S., Chemsseddoha, A., Saquaque, A., 1989. Les plutons granitiques tardi carbonifères marqueurs de la déformation crustale. L'exemple des granitoïdes de la méseta marocaine. Comptes Rendus de l'Académie des sciences, Série II, 309, 291–296.

Lardeaux, J.-M., Schulmann, K., Faure, M., Janoušek, V., Lexa, O., Skrzypek, E., Edel, J.-B. and Štípská, P., 2014. The moldanubian zone in the French Massif Central, Vosges/Schwarzwald and Bohemian Massif revisited: differences and similarities. Geological Society, London, Special Publications, 405(1), 7–44. http://dx.doi.org/10.1144/SP405.14,

Letsch, D., El Houicha, M., von Quadt, A., Winkler, W., 2018. A missing link in the peri-Gondwanan terrane collage: The Precambrian basement of the Moroccan Meseta and its lower Paleozoic cover. Canadian Journal of Earth Sciences, 55, 33–51. https://doi.org/10.1139/cjes-2017-0086

Lindner, M., Dörr, W., Reither, D., Finger, F., 2021. The Dobra Gneiss and the Drosendorf Unit in the southeastern Bohemian Massif, Austria: West Amazonian crust in the heart of Europe. Geological Society, London, Special Publications, 503, 185–207. https://doi.org/10.1144/SP503-2019-232

Martínez Catalán, J.R., Schulmann, K., Ghienne, J.F., 2021. The Mid-Variscan Allochthon: Keys from correlation, partial retro deformation and plate-tectonic reconstruction to unlock the geometry of a non-cylindrical belt. Earth-Science Reviews, 220. https://doi.org/10.1016/j.earscirev.2021.103700

Matthews, K.J., Maloney, K.T., Zahirovic, S., Williams, S.E., Seton, M., Müller, R.D., 2016. Global plate boundary evolution and kinematics since the late Paleozoic. Global and Planetary Change, 146, 226–250. https://doi.org/10.1016/j.gloplacha.2016.10.002

Mazur, S., Kröner, A., Szczepański, J., Turniak, K., Hanžl, P., Melichar, R., Rodionov, N. V., Paderin, I., Sergeev, S.A., 2010. Single zircon U-Pb ages and geochemistry of granitoid gneisses from SW Poland: Evidence for an Avalonian affinity of the Brunian microcontinent. Geological Magazine, 147, 508–526. https://doi.org/10.1017/S001675680999080X

Michard, A., 1982. Le massif Paléozoïque des Rehamna (Maroc) : Stratigraphie, Tectonique et Petrogenese d'un segment de la Chaine Varisque. Notes et Mémoires du Service Géologique du Maroc, Rabat, 303, 1–180.

Michard, A., Soulaimani, A., Hoepffner, C., Ouanaimi, H., Baidder, L., Rjimati, E.C., Saddiqi, O., 2010. The South-Western Branch of the Variscan Belt: Evidence from Morocco. Tectonophysics, 492 (1–4), 1–24. https://doi.org/10.1016/j.tecto.2010.05.021

Moreno, C., Sáez, R., González, F., Almodóvar, G., Toscano, M., Playford, G., Alansari, A., Rziki, S., Bajddi, A., 2008. Age and depositional environment of the Draa Sfar massive sulfide deposit, Morocco. Mineralium Deposita, 43, 891–911. https://doi.org/10.1007/s00126-008-0199-x

Nemchin, A.A., Cawood, P.A., 2005. Discordance of the U–Pb system in detrital zircons: Implication for provenance studies of sedimentary rocks. Sedimentary Geology, 182, 143–162. https://doi.org/10.1016/j.sedgeo.2005.07.011

Oriolo, S., Schulz, B., Geuna, S., González, P. D., Otamendi, J. E., Sláma, J., Druguet, E., Siegesmund, S., 2021. Early Paleozoic accretionary orogens along the Western Gondwana margin. Geoscience Frontiers, 12 (1), 109–130. https://doi.org/10.1016/j.gsf.2020.07.001

Pereira, M.F., El Houicha, M., Aghzer, A., Silva, J.B., Linnemann, U., Jouhari, A., 2014. New U-Pb zircon dating of late Neoproterozoic magmatism in Western Meseta (Morocco). Gondwana 15 - North meets South. 133.

Pereira, M.F., El Houicha, M., Chichorro, M., Armstrong, R., Jouhari, A., El Attari, A., Ennih, N., Silva, J.B., 2015. Evidence of a Paleoproterozoic basement in the Moroccan Variscan belt (Rehamna Massif, Western Meseta). Precambrian Research, 268, 61–73. https://doi.org/10.1016/j.precamres.2015.07.010

Pérez-Cáceres, I., Martínez Poyatos, D., Simancas, J.F., Azor, A., 2017. Testing the Avalonian affinity of the South Portuguese Zone and the Neoproterozoic evolution of SW Iberia through detrital zircon populations. Gondwana Research, 42, 177–192. https://doi.org/10.1016/j.gr.2016.10.010

Perez, N.D., Teixell, A., Gómez-Gras, D., Stockli, D.F., 2019. Reconstructing Extensional Basin Architecture and Provenance in the Marrakech High Atlas of Morocco: Implications for Rift Basins and Inversion Tectonics. Tectonics, 38, 1584–1608. https://doi.org/10.1029/2018TC005413

Piqué, A., Jeannette, D., Michard, A., 1980. The Western Meseta Shear Zone, a major and permanent feature of the Hercynian belt of Morocco. Journal of Structural Geology, 2(1–2), 55–61. https://doi.org/10.1016/0191-8141(80)90034-6

Piqué, A., Bossière, G., Bouillin, J.-P., Chalouan, A., Hoepffner, C., 1993a. Southern margin of the Variscan belt: the north-western Gondwana mobile zone (eastern Morocco and Northern Algeria). Geologische Rundschau, 82, 432–439. https://doi.org/10.1007/BF00212407

Piqué, A., El Hassani, A., Hoepffner C., 1993b. Les déformations ordoviciennes dans la zone des Sehoul (Maroc septentrional) : une orogenèse calédonienne en Afrique du Nord. Canadian Journal of Earth Sciences, 30(7), 1332–1337. https://doi.org/10.1139/e93-114

Razin, P., Baudin, T., Chèvremont, P., Andries, D., Youbi, N.A., Hoepffner, C., Thiéblemont, D., Chihani, E.M., 2003. Carte géologique du Maroc au 1/50 000, feuille de Jebel Kharrou, Mémoire explicatif. Notes et Mémoires du Service Géologique du Maroc, Rabat 436 bis, 1–105.

Reiners, P.W., Carlson, R.W., Renne, P.R., Cooper, K.M., Granger, D.E., McLean, N.M., Schoene, B., 2017. Geochronology and thermochronology, John Wiley & Sons Ltd, 1–464. https://doi.org/10.1002/9781118455876

688 Ribeiro, A., Munhá, J., Dias, R., Mateus, A., Pereira, E., Ribeiro, L., Fonseca, P., Araújo, A.,
689 Oliveira, T., Romão, J., Chaminé, H., Coke, C., Pedro, J., 2007. Geodynamic evolution
690 of the SW Europe Variscides. Tectonics, 26, TC6009.
691 https://doi.org/10.1029/2006TC002058
692 Rubatto, D. 2002. Zircon trace element geochemistry: Partitioning with garnet and the link
693 between U–Pb ages and metamorphism. Chemical Geology, 184, 123–138.
694 https://doi.org/10.1016/S0009-2541(01)00355-2
695 Simancas, J.F., Tahiri, A., Azor, A., Lodeiro, F.G., Poyatos, D.J.M., 2005. The tectonic frame
696 of the Variscan–Alleghanian orogen in Southern Europe and Northern Africa.
697 Tectonophysics, 398, 181–198. https://doi.org/10.1016/j.tecto.2005.02.006
698 Simancas, J.F., Azor, A., Martínez-Poyatos, D., Tahiri, A., El Hadi, H., González-Lodeiro, F.,
699 Pérez-Estaún, A., Carbonell, R., 2009. Tectonic relationships of Southwest Iberia with
700 the allochthons of Northwest Iberia and the Moroccan Variscides. Comptes Rendus
701 Geoscience, 341, 103–113. http://dx.doi.org/10.1016/j.crte.2008.11.003
702 Sláma, J., Kosler, J., Condon, D.J., Crowley, J.L., Gerdes, A., Hanchar, J.M., Horstwood,
703 M.S.A., Morris, G.A., Nasdala, L., Norberg, N., Schaltegger, U., Schoene, B., Tubrett,
704 M.N., Whitehouse, M.J., 2008. Plesovice zircon - A new natural reference material for
705 U-Pb and Hf isotopic microanalysis. Chemical Geology, 249, 1–35.
706 https://doi.org/10.1016/j.chemgeo.2007.11.005
707 Spencer, C.J., Kirkland, C.L., Taylor, R.J.M., 2016. Strategies towards statistically robust
708 interpretations of in situ U–Pb zircon geochronology. Geoscience Frontiers, 7, 581–589.
709 https://doi.org/10.1016/j.gsf.2015.11.006
710 Stampfli, G.M., Borel, G.D., 2002. A plate tectonic model for the Paleozoic and Mesozoic
711 constrained by dynamic plate boundaries and restored synthetic oceanic isochrons. Earth
712 and Planetary Science Letters, 196, 17–33. https://doi.org/10.1016/S0012-
713 821X(01)00588-X
714 Stampfli, G.M., Vavassis, I., De Bono, A., Rosselet, F., Matti, B., Bellini, M., 2003. Remnants
715 of the paleotethys oceanic suture-zone in the western tethyan area. Bollettino della
716 Società Geologica Italiana, 2, 1–23.
717 Stampfli, G.M., Hochard, C., Vérard, C., Wilhem, C., VonRaumer, J., 2013. The formation of
718 Pangea. Tectonophysics, 593, 1–19. https://doi.org/10.1016/j.tecto.2013.02.037
719 Tahiri, A., Montero, P., El Hadi, H., Martínez Poyatos, D., Azor, A., Bea, F., Simancas, J.F.,
720 González Lodeiro, F., 2010. Geochronological data on the Rabat-Tiflet granitoids: Their
721 bearing on the tectonics of the Moroccan Variscides. Journal of African Earth Sciences,
722 57, 1–13. https://doi.org/10.1016/j.jafrearsci.2009.07.005
723 Thomas, W.A., 2011. Detrital-zircon geochronology and sedimentary provenance. Lithosphere,
724 3, 304–308. https://doi.org/10.1130/RF.L001.1
725 Vermeesch, P., 2004. How many grains are needed for a provenance study? Earth and Planetary
726 Science Letters, 224, 441–451. https://doi.org/10.1016/j.epsl.2004.05.037
727 Vermeesch, P., 2018. IsoplotR: A free and open toolbox for geochronology. Geoscience
728 Frontiers, 9, 1479–1493. https://doi.org/10.1016/j.gsf.2018.04.001
729 Wernert, P., Schulmann, K., Chopin, F., Štípská, P., Bosch, D., El Houicha, M., 2016.
730 Tectonometamorphic evolution of an intracontinental orogeny inferred from P–T–t–d
731 paths of the metapelites from the Rehamna massif (Morocco). Journal of Metamorphic
732 Geology, 34, 917–940. https://doi.org/10.1111/jmg.12214
733 Wiedenbeck, M., Allé, P., Corfu, F., Griffin, W.L., Meier, M., Oberli, F., Von Quadt, A.,
734 Roddick, J.C., Spiegel, W., 1995. Three natural zircon standards for U-Th-Pb, Lu-Hf,
735 trace element and REE analyses. Geostandards Newsletter, 19, 1–23.
736 https://doi.org/10.1111/j.1751-908X.1995.tb00147.x

737 Zimmermann, S., Mark, C., Chew, D., Voice, P.J., 2018. Maximising data and precision from
738 detrital zircon U-Pb analysis by LA-ICPMS: The use of core-rim ages and the single-
739 analysis concordia age. Sedimentary Geology, 375, 5–13.
740 https://doi.org/10.1016/j.sedgeo.2017.12.020

Figure Caption

Fig. **1.** Simplified geological map of the Moroccan Variscides (modified after Hoepffner *et al.*, 2005; Michard *et al*., 2010 in Chopin *et al*., 2014). Middle Meseta Fault Zone (MMFZ), Western Meseta Shear Zone (WMSZ), South Meseta Fault (SMF), South Meseta Front (SMFr), South Atlas Fault (SAF), Rabat-Tiflet Fault Zone (RTFZ), Sidi Bettache B~~b~~asin (SBB), and Azrou-Khenifra Basin (AKB).

Fig. 2. Simplified Geological map of the Rehamna massif (adapted from Corsini, 1988; Baudin *et al.*, 2003; Chopin *et a*l., 2014; Pereira *et al.*, 2015; El Houicha *et al*., 2018).

Fig. 3. Synthetic lithostratigraphic logs of the Rehamna massif subdivided into the Western (i.e., Coastal Block), Central and Eastern Rehamna, and the lower and upper metamorphic units (modified after Michard, 1982; Hoepffner, 1974; Corsini *et al.*, 1988; Baudin *et al.*, 2003; Chopin *et al.*, 2014; Pereira *et al.*, 2015; El Houicha *et al.*, 2018).

Fig. 4. Field photographs of the sample location. (a) A quarry at the southwest of the Sebt Brikyine granite showing the Paleoproterozoic basement and its early Cambrian sedimentary cover (modified after Pereira *et al.*, 2015); (b) Basal early Cambrian microbrecia/(meta)arkose (R161-A); (c) Panorama of a quarzitic layer from the Skhour Formation at Koudiat Karkaba (SK1-Z); (d) Cross section and (e) field photograph of the Ouled Zednes Fault Zone (modified after Jenny, 1974) with location of the sample R255-OZ and location of the Eifelian-Frasnian corals from El Houicha *et al.* (2019); (f) Sandstone (R255-OZ); (g) Quartzite from the Ouled Hassine-Ouled Zednes Formation at Souq el Had (R257-OH); (h) Dalaat Formation; (i) Detail of the Dalaat Formation showing layered (calcareous)sandstone (R256-DT).

Fig. 5. (a-e) Microphotographs of the samples R16-1A, SK1-Z, R255-OZ, R257-OH and R256-DT. Mineral abbreviations: Qtz: quartz, Ms: white micas, Cal: calcite.

Fig. 6. Cathodoluminescence images of selected zircon grains.

765 **Fig. 7.** (a) Concordia diagrams of the sample R16-1A. Green circles (concordant); Gray circles
766 (discordant); (b) Zircon U–Pb Kernel Density Estimator (KDE) diagrams for the sample R16-
767 1A. Red dots indicate Th/U ratios.
768 **Fig. 8.** (a) Concordia diagrams, zircon U–Pb Kernel Density Estimation (KDE) diagrams and
769 percentage of different population age groups for the samples (a) SK1-Z, (b) R257-OH, (c)
770 R255-OZ and (d) R256-DT. Red circles (concordant); Gray circles (discordant).
771 **Fig. 9.** Conceptual tectonic and sediment dispersal evolution of the Rehamna massif during the
772 (a) early Cambrian (see El Houicha *et al.*, 2018 for more details), (b) Ordovician, (c) Devonian
773 and (d) early Carboniferous (coeval tectonic structures are omitted). Black arrows represent
774 sourcing properly identified in our zircon age spectra, while grey arrows represent hypothesized
775 and later remobilized sourcing only found in younger zircon age spectra.
776 **Fig. 10.** Paleogeographic reconstruction (modified after Martinez Catalan *et al.,* 2021) showing
777 probable Ordovician to early Carboniferous sources for clastic sediments sampled in the
778 Rehamna massif.
779 **Table 1.** List of samples with details of the analyses carried out on the zircon grains.
780

Fig. 1.

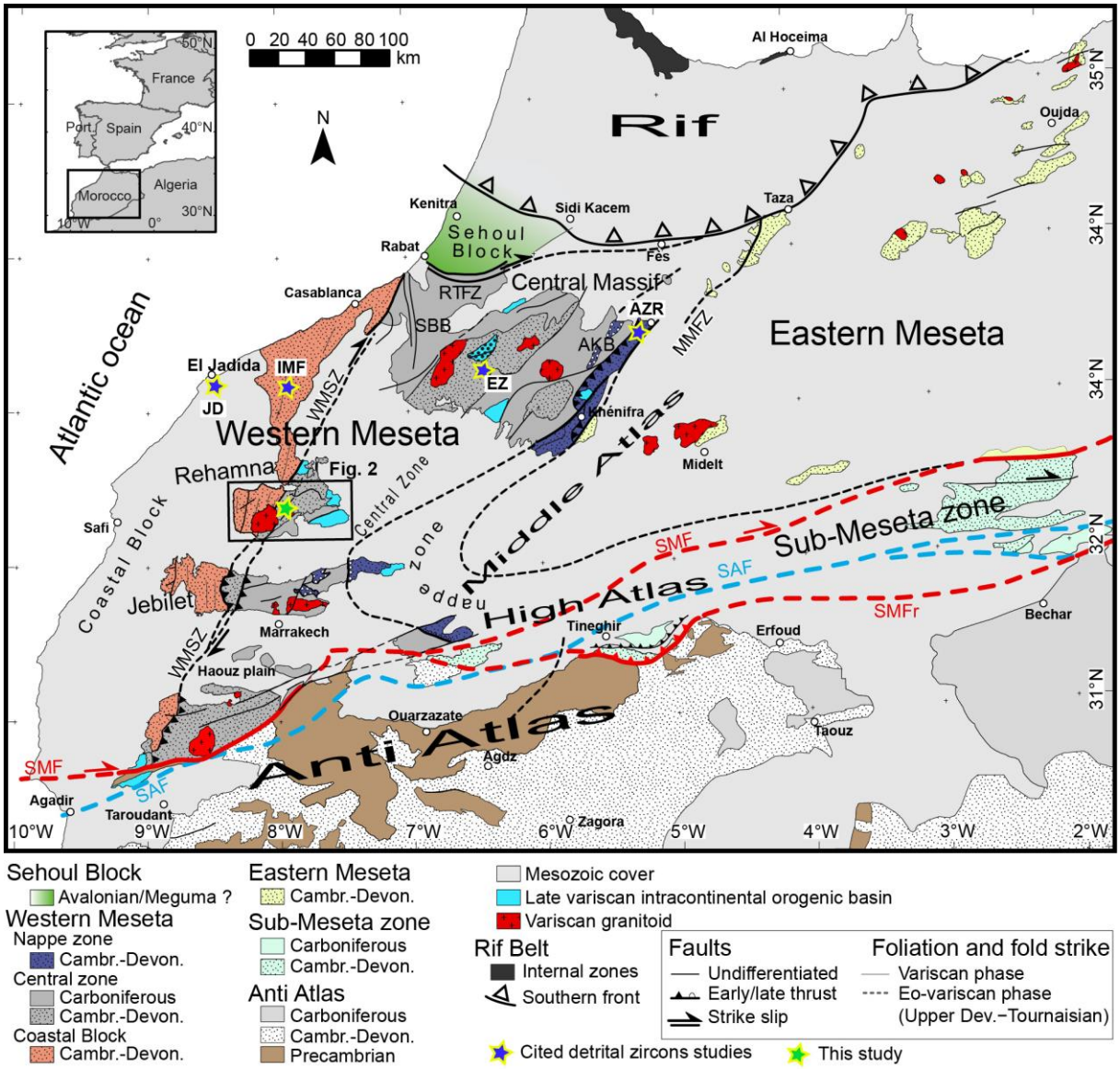
0 20 40 60 80 100 km
N
Rif
Al Hoceima
Oujda
Taza
Kenitra
Sidi Kacem
Rabat
Sehoul Block
Fès
Casablanca
RTFZ
Central Massif
AZR
SBB
AKB
MMFZ
Eastern Meseta
Atlantic ocean
El Jadida
IMF
JD
WMSZ
EZ
Western Meseta
Khénifra
Middle Atlas
Rehamna
Fig. 2
Midelt
Central Zone
Safi
Coastal Block
Jebilet
Sub-Meseta zone
SMF
SAF
SMFr
Marrakech
High Atlas
Tinejdad
Erfoud
Bechar
Haouz plain
Ouarzazate
Anti Atlas
Agdz
Taouz
Agadir
Taroudant
Zagora
10°W
9°W
8°W
7°W
6°W
5°W
4°W
3°W
2°W
35°N
34°N
32°N
31°N
Sehoul Block
Avalonian/Meguma ?
Western Meseta
Nappe zone
Cambr.-Devon.
Central zone
Carboniferous
Cambr.-Devon.
Coastal Block
Cambr.-Devon.
Eastern Meseta
Cambr.-Devon.
Sub-Meseta zone
Carboniferous
Cambr.-Devon.
Anti Atlas
Carboniferous
Cambr.-Devon.
Precambrian
Mesozoic cover
Late variscan intracontinental orogenic basin
Variscan granitoid
Rif Belt
Internal zones
Southern front
Faults
Undifferentiated
Early/late thrust
Strike slip
Foliation and fold strike
Variscan phase
Eo-variscan phase
(Upper Dev.–Tournaisian)
Cited detrital zircons studies
This study

784 **Fig. 2.**

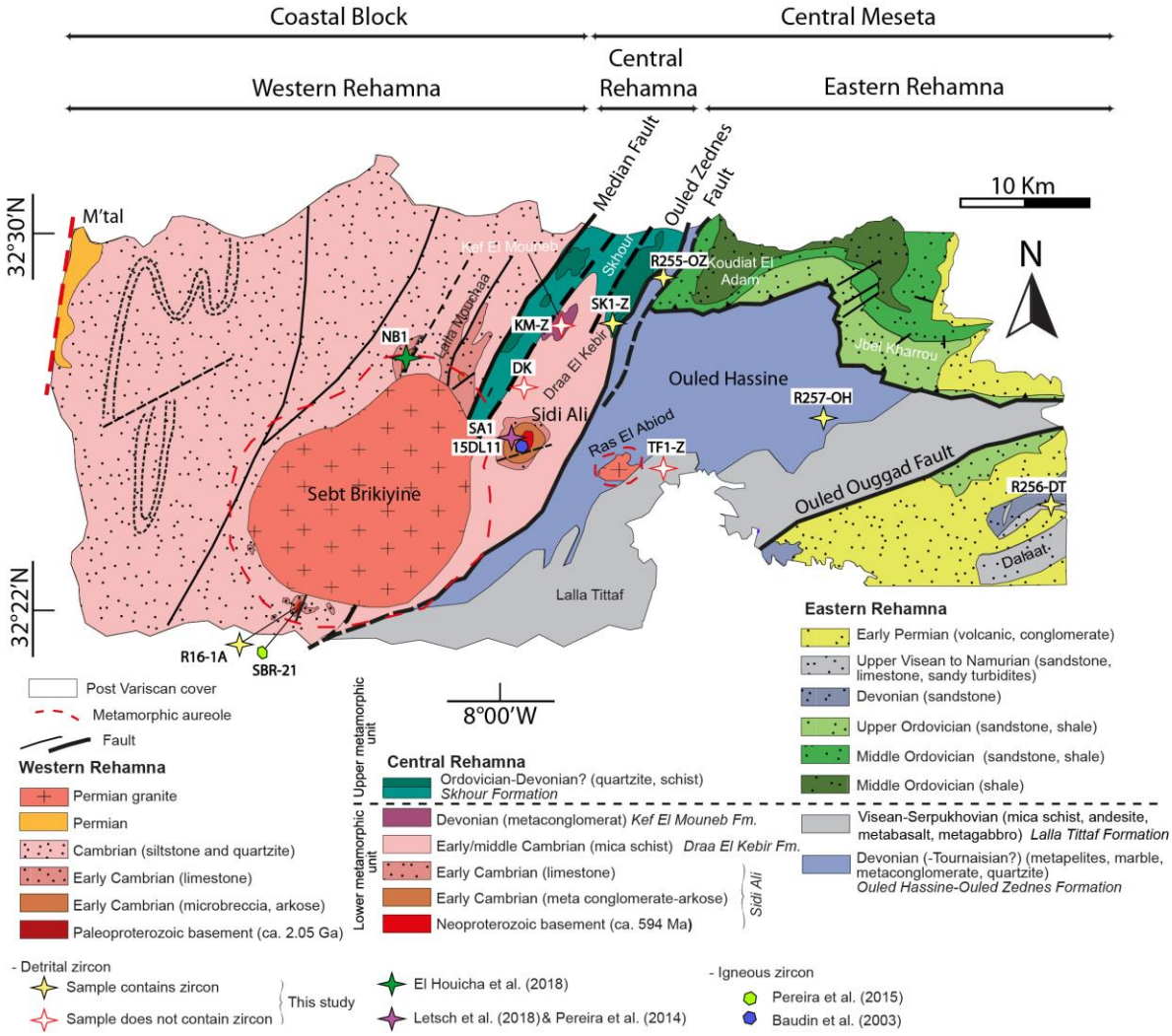

785

786

787 **Fig. 3.**

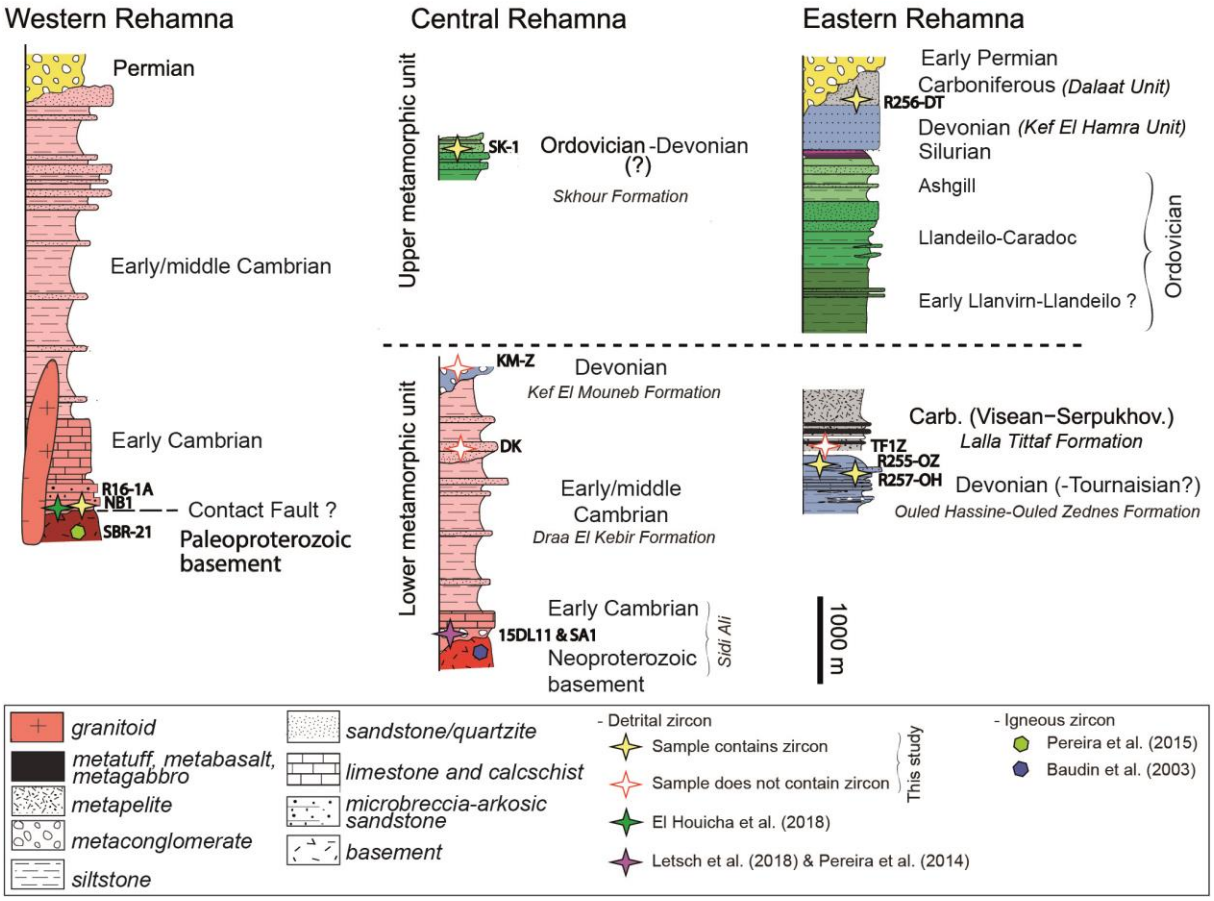

788

789

790 **Fig. 4.**

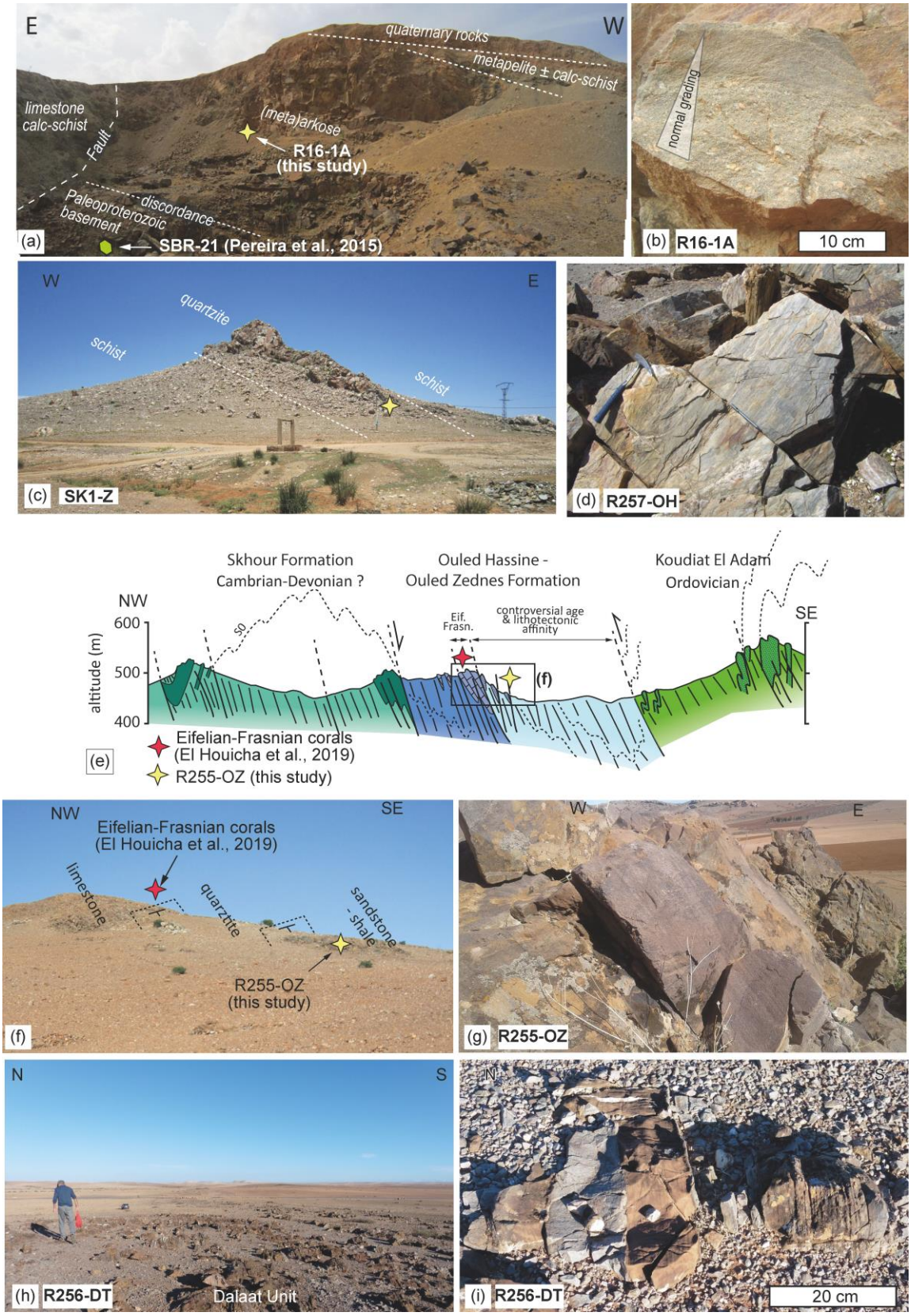
E
W
quaternary rocks
metapelite ± calc-schist
limestone
calc-schist
Fault
(meta)arkose
R16-1A
(this study)
Paleoproterozoic
basement
discordance
(a)
SBR-21 (Pereira et al., 2015)
normal grading
(b) R16-1A
10 cm
W
E
quartzite
schist
schist
(c) SK1-Z
(d) R257-OH
Skhour Formation
Cambrian-Devonian ?
Ouled Hassine -
Ouled Zednes Formation
Koudiat El Adam
Ordovician
NW
SE
600
500
400
altitude (m)
S0
Eif.
Frasn.
controversial age
& lithotectonic
affinity
(f)
Eifelian-Frasnian corals
(El Houicha et al., 2019)
R255-OZ (this study)
(e)
NW
SE
Eifelian-Frasnian corals
(El Houicha et al., 2019)
limestone
quarztite
sandstone
- shale
R255-OZ
(this study)
(f)
W
E
(g) R255-OZ
N
S
(h) R256-DT
Dalaat Unit
N
S
(i) R256-DT
20 cm

791

Fig. 5.

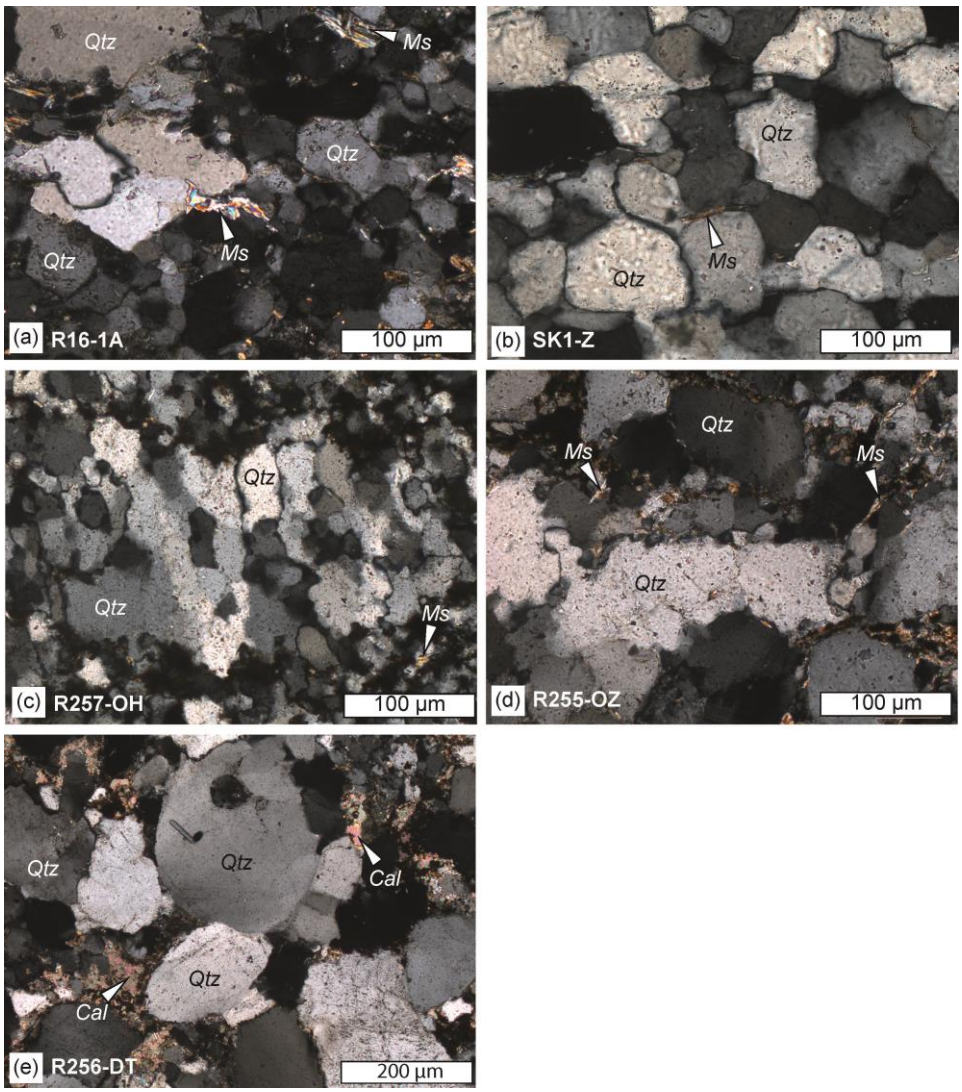
Qtz
Ms
Qtz
Ms
Qtz
(a) R16-1A
100 µm
Qtz
Ms
Qtz
(b) SK1-Z
100 µm
Qtz
Qtz
Ms
(c) R257-OH
100 µm
Qtz
Ms
Ms
Qtz
(d) R255-OZ
100 µm
Qtz
Qtz
Cal
Qtz
Cal
(e) R256-DT
200 µm

794 **Fig. 6.**

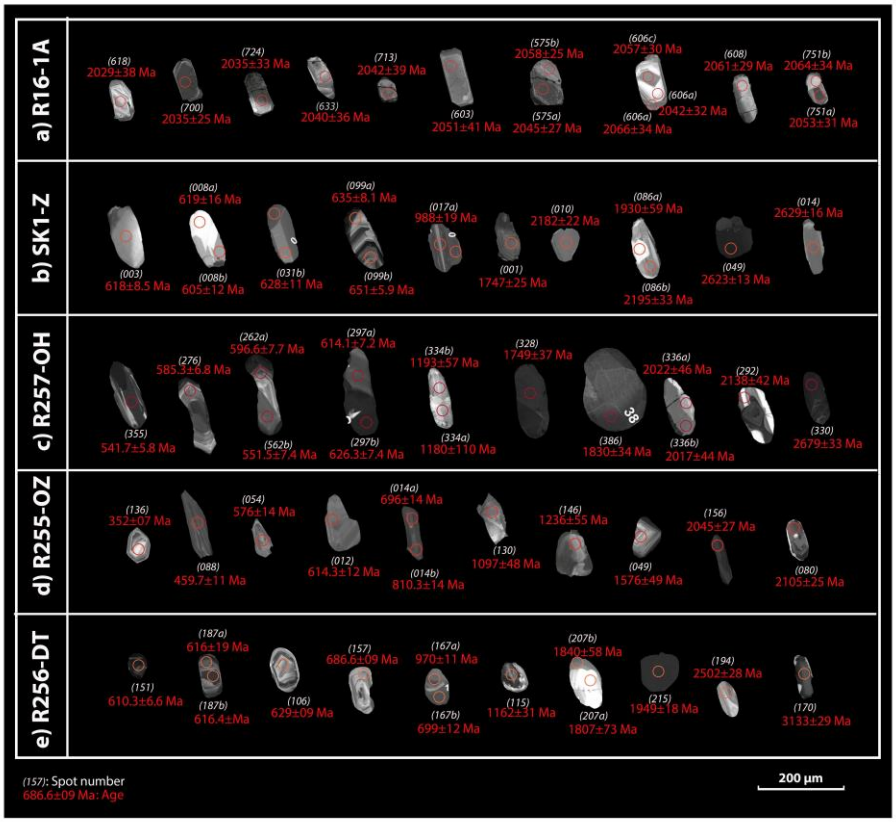
a) R16-1A
(618) 2029±38 Ma
(700) 2035±25 Ma
(724) 2035±33 Ma
(633) 2040±36 Ma
(713) 2042±39 Ma
(603) 2051±41 Ma
(575b) 2058±25 Ma
(575a) 2045±27 Ma
(606c) 2057±30 Ma
(606a) 2042±32 Ma
(606a) 2066±34 Ma
(608) 2061±29 Ma
(751b) 2064±34 Ma
(751a) 2053±31 Ma
b) SK1-Z
(003) 618±8.5 Ma
(008a) 619±16 Ma
(008b) 605±12 Ma
(031b) 628±11 Ma
(099a) 635±8.1 Ma
(099b) 651±5.9 Ma
(017a) 988±19 Ma
(001) 1747±25 Ma
(010) 2182±22 Ma
(086a) 1930±59 Ma
(086b) 2195±33 Ma
(049) 2623±13 Ma
(014) 2629±16 Ma
c) R257-OH
(355) 541.7±5.8 Ma
(276) 585.3±6.8 Ma
(262a) 596.6±7.7 Ma
(562b) 551.3±7.4 Ma
(297a) 614.1±7.2 Ma
(297b) 626.3±7.4 Ma
(334b) 1193±57 Ma
(334a) 1180±110 Ma
(328) 1749±37 Ma
(386) 1830±34 Ma
(336a) 2022±46 Ma
(336b) 2017±44 Ma
(292) 2138±42 Ma
(330) 2679±33 Ma
d) R255-OZ
(136) 352±07 Ma
(088) 459.7±11 Ma
(054) 576±14 Ma
(012) 614.3±12 Ma
(014a) 696±14 Ma
(014b) 810.3±14 Ma
(130) 1097±48 Ma
(146) 1236±55 Ma
(049) 1576±49 Ma
(156) 2045±27 Ma
(080) 2105±25 Ma
e) R256-DT
(151) 610.3±6.6 Ma
(187a) 616±19 Ma
(187b) 616.4±Ma
(106) 629±09 Ma
(157) 686.6±09 Ma
(167a) 970±11 Ma
(167b) 699±12 Ma
(115) 1162±31 Ma
(207b) 1840±58 Ma
(207a) 1807±73 Ma
(215) 1949±18 Ma
(194) 2502±28 Ma
(170) 3133±29 Ma
(157): Spot number
686.6±09 Ma: Age
200 µm

795

Fig. 7.

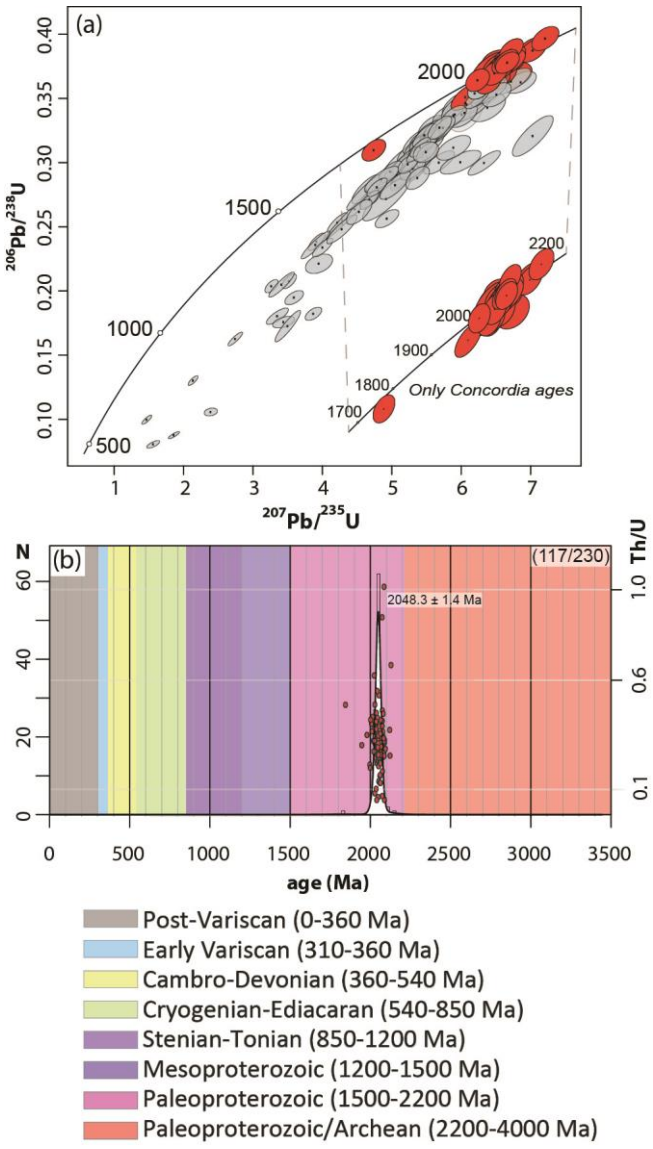
(a)
2000
1500
1000
500
2200
2000
1900
1800
1700
Only Concordia ages
$^{206}Pb/^{238}U$
$^{207}Pb/^{235}U$
(b)
(117/230)
2048.3 ± 1.4 Ma
N
Th/U
age (Ma)
Post-Variscan (0-360 Ma)
Early Variscan (310-360 Ma)
Cambro-Devonian (360-540 Ma)
Cryogenian-Ediacaran (540-850 Ma)
Stenian-Tonian (850-1200 Ma)
Mesoproterozoic (1200-1500 Ma)
Paleoproterozoic (1500-2200 Ma)
Paleoproterozoic/Archean (2200-4000 Ma)

798 **Fig. 8.**

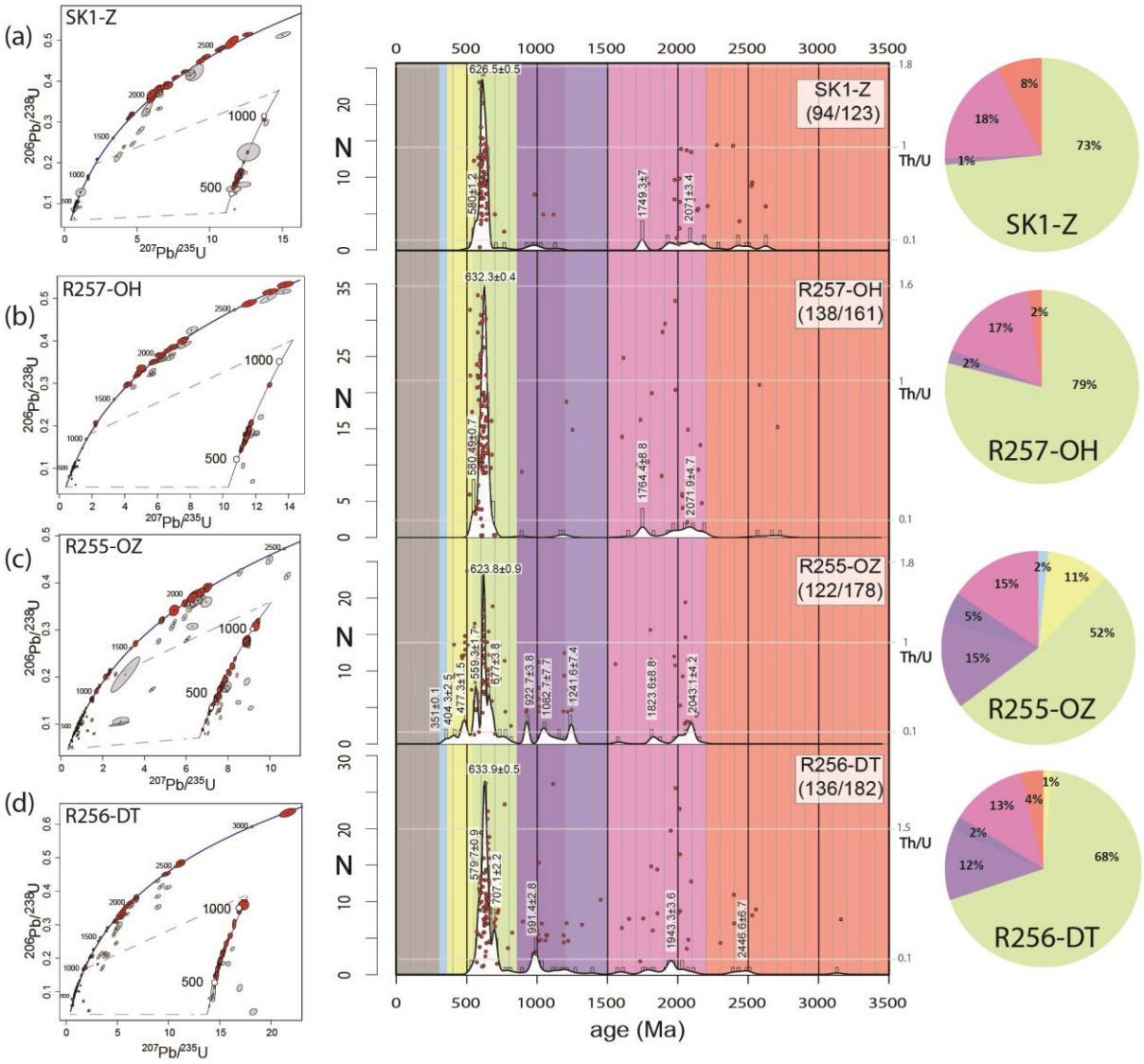

799

800

801 **Fig. 9.**

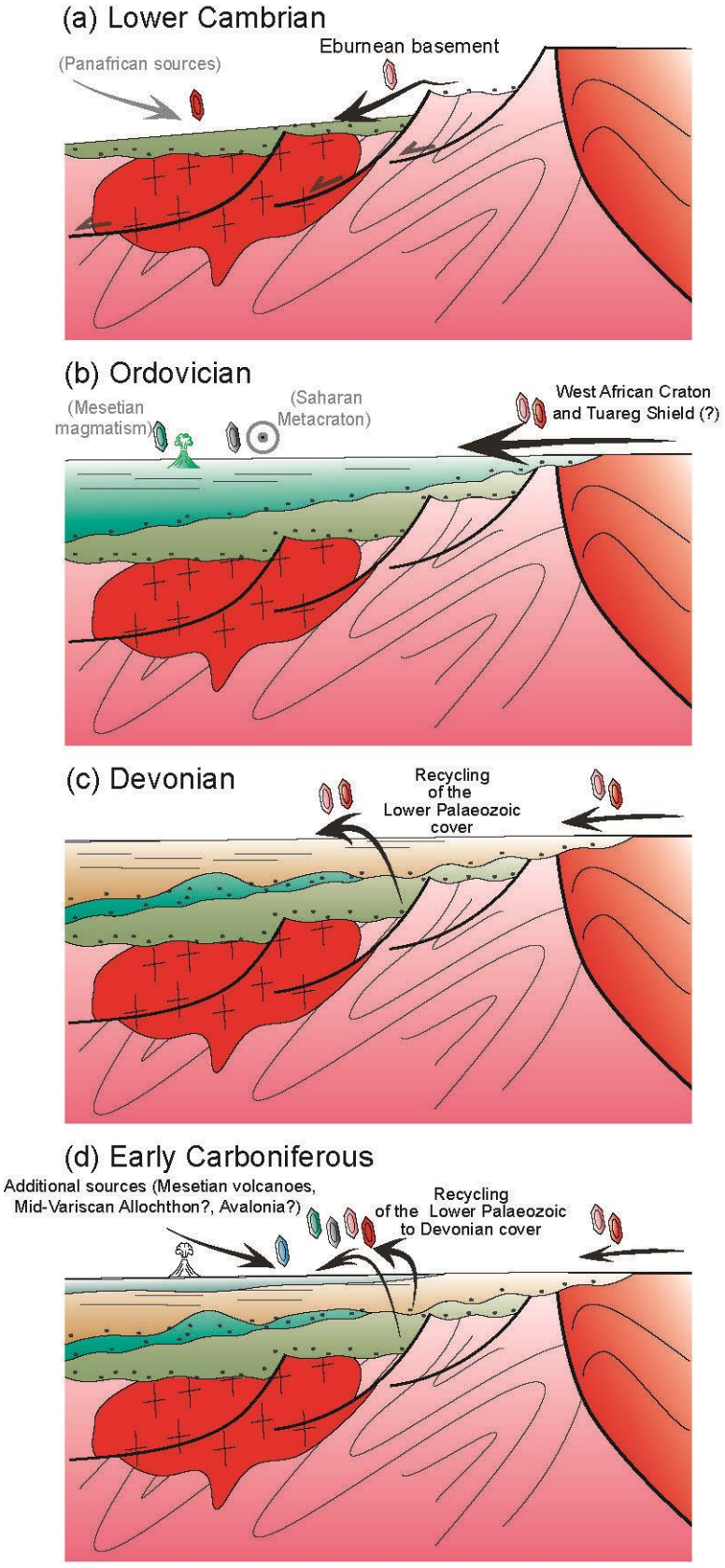
(a) Lower Cambrian
(Panafrican sources)
Eburnean basement
(b) Ordovician
(Mesetian magmatism)
(Saharan Metacraton)
West African Craton and Tuareg Shield (?)
(c) Devonian
Recycling of the Lower Palaeozoic cover
(d) Early Carboniferous
Additional sources (Mesetian volcanoes, Mid-Variscan Allochthon?, Avalonia?)
Recycling of the Lower Palaeozoic to Devonian cover

802

803 **Fig. 10.**

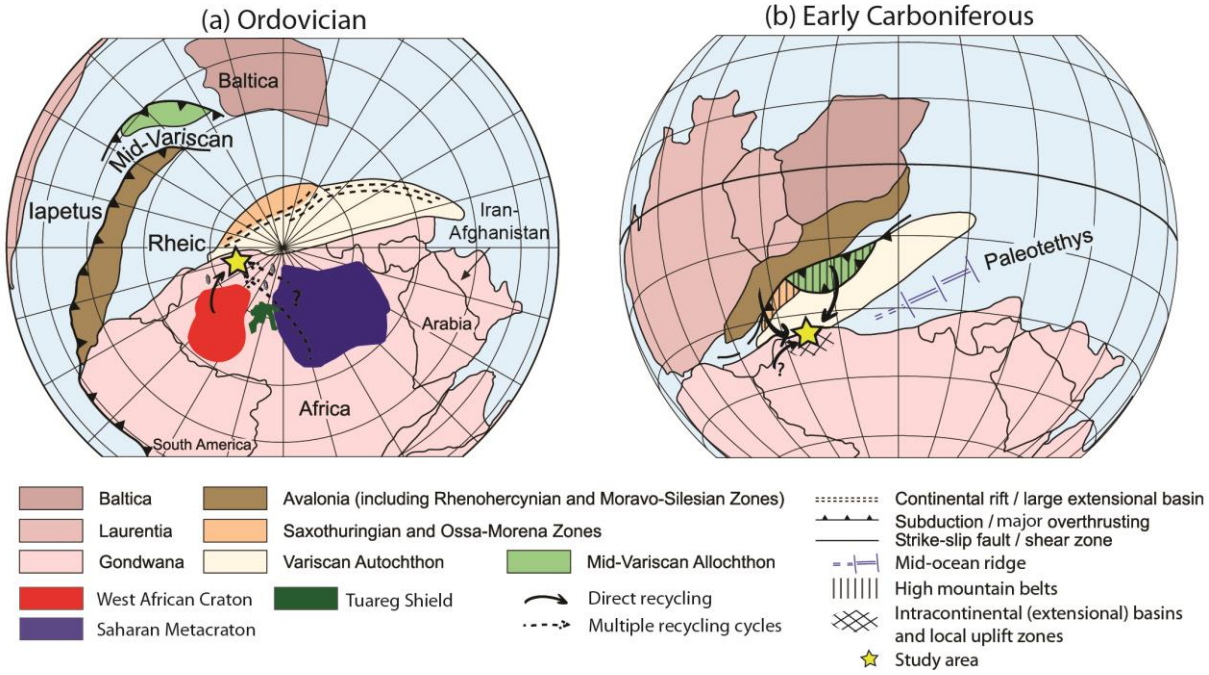

804

805 **Tab1e 1:**

Block/Unit/Formation	Site	Sample	Long.	Lat.	Lithostratigraphy (from literature)	Sample's age (this study)	Lithology	Zircon grains analyzed	Number of concordant analyses/ Number of analyses
Dalaat unit	Dalaat formation	**R256-DL**	-7.523870	32.337190	Middle (?)-late Visean (Razin et al., 2003)	idem	sandstone	175	136/182
Ouled Hassine-Ouled Zednes	Jaafra	**R257-OH**	-7.730770	32.373330	Lower or Middle to Upper Devonian (e.g. Hoepffner 1974; Comée, 1982; Razin et al., 2003)	idem	quartzitic lense	173	138/161
Lalla Tittaf	Imi	**TF1Z**	-7.865546	32.336293	Carboniferous (?) (Hoepffner et al., 1974)	idem	quartzite interlayerd in mica schist	no zircon	no zircon
Ouled Hassine-Ouled Zednes	Ouled Zednes Fault Zone	**R255-OZ**	-7.850210	32.484050	Upper Devonian (post-Frasnian) to Dinantian (Jenny, 1974; Baudin et al., 2002; Razin 2003) Cambro-Ordovician or Upper Devonian (Baudin et al., 2003; Razin, 2003)	Tournaisian (maximum depositional age)	quartzitic lense	292	122/178
Kef El Mouneb	Kef El Mouneb	**KM-Z**	-7.949580	32.427268	Devonian (?) (Destombes et al., 1982, Baudin et al., 2003)	idem	coarse meta-conglomerate	no zircon	no zircon
Skhour	Koudiat Karkaba	**SK1-Z**	-7.899843	32.439914	Ordovician-Devonian (?) (Baudin et al., 2003)	Ordovician	quartzite	99	94/123
Draa el Kebir	Draa el Kebir	**DK**	-7.986895	32.386054	Middle Cambrian (?) (Corsini et al., 1988)	idem	quartzite interlayerd in mica schist	no zircon	no zircon
Coastal block	SW of the Sebt Brikiyine granite	**Rt6-1A**	-8.172580	32.226670	Early Cambrian (Corsini et al., 1988)	idem	arkose-sandtone	196	117/230

806